Vol. 43 — N° 4 12 19 p. 543 – 565

GEOSTANDARDS and GEOANALYTICAL RESEARCH

In Situ U-Th-Pb Dating and Sr-Nd Isotope Analysis of Bastnäsite by LA-(MC)-ICP-MS

Yue-Heng **Yang** (1, 2)*, Fu-Yuan **Wu** (1, 2), Qiu-Li **Li** (1, 2), Yamirka **Rojas-Agramonte** (3, 4), Jin-Hui **Yang** (1, 2), Yang **Li** (1, 2, 5), Qian **Ma** (1, 2, 6), Lie-Wen **Xie** (1, 2), Chao **Huang** (1, 2), Hong-Rui **Fan** (1, 2), Zi-Fu **Zhao** (7) and Cheng **Xu** (8)

(1) State Key Laboratory of Lithospheric Evolution, Institute of Geology and Geophysics, Chinese Academy of Sciences, P. B. 9825, Beijing, 100029, China
(2) Innovation Academy of Earth Science, Chinese Academy of Sciences, Beijing, 100029, China
(3) Institut für Geowissenschaften, Johannes Gutenberg-Universität, Becherweg 21, Mainz, 55099, Germany
(4) Universidad de los Andes, Cra 1 No 18A – 70, Bogotá, M1-307, Colombia
(5) Faculty of Geography and Resources Sciences, Sichuan Normal University, Chengdu, 610068, China
(6) State Key Laboratory of Geological Processes and Mineral Resources, School of Earth Science and Resources, China University of Geosciences, Beijing, 100083, China
(7) CAS Key Laboratory of Crust-Mantle Materials and Environments, School of Earth and Space Science, University of Science and Technology of China, Hefei, 230026, China
(8) Laboratory of Orogenic Belts and Crustal Evolution, School of Earth and Space Sciences, Peking University, Beijing, 100871, China
* Corresponding author. e-mail: yangyueheng@mail.iggcas.ac.cn

Bastnäsite is the end member of a large group of carbonate–fluoride minerals with the common formula (REE) $CO_3F{\cdot}CaCO_3$. This group is generally widespread and, despite never occurring in large quantities, represents the major economic light rare earth element (LREE) mineral in deposits related to carbonatite and alkaline intrusions. Since bastnäsite is easily altered and commonly contains inclusions of earlier-crystallised minerals, *in situ* analysis is considered the most suitable method to measure its U-Th-Pb and Sr-Nd isotopic compositions. Electron probe microanalysis and laser ablation (multi-collector) inductively coupled plasma-mass spectrometry of forty-six bastnäsite samples from LREE deposits in China, Pakistan, Sweden, Mongolia, USA, Malawi and Madagascar indicate that this mineral typically has high Th and LREE and moderate U and Sr contents. Analysis of an in-house bastnäsite reference material (K-9) demonstrated that precise and accurate U-Th-Pb ages could be obtained after common Pb correction. Moreover, the Th-Pb age with its high precision is preferable to the U-Pb age because most bastnäsites have relatively high Th rather than U contents. These results will have significant implications for understanding the genesis of endogenous ore deposits and formation processes related to metallogenic geochronology research.

Keywords: bastnäsite, U-Th-Pb ages, Sr-Nd isotopes, laser ablation, LREE, carbonatite.

Received 19 Nov 18 – Accepted 09 Aug 19

The ability to accurately date the time of mineralisation is crucial for understanding the genesis of endogenous ore deposits and/or ore-forming processes (Robert 1990). Numerous radio-isotopic methods have been used widely to date mineralisation processes including K (Ar)-Ar, Rb-Sr, Sm-Nd, Lu-Hf, Re-Os and U-Pb techniques. Successful attempts have been reported previously [e.g., Che *et al.* (2015, Re-Os dating of molybdenite, U-Pb dating of columbite–tantalite), Romer and Luders (2006, U-Pb dating of columbite), Gulson and Jones (1992, cassiterite), Anglin *et al.* (1996, Sm-Nd dating of scheelite) and Nakai *et al.* (1990, Rb-Sr dating of sphalerite)). Among them, the U-Pb method has been generally considered as the most powerful technique to obtain precise and accurate ages because of the two independent decay schemes and their concordance. Nevertheless, this method cannot be used for metal ore deposits because of the very low U content in most metal ore minerals. This problem is also encountered when dating major economic rare earth element (REE) deposits that are generally related to the occurrence of alkaline and

doi: 10.1111/ggr.12297

carbonatite rocks (Sal'Nikova *et al.* 2010). In such cases, it is more suitable to date minerals in gangue veins intruding ore deposits.

Bastnäsite can be used to circumvent the problems mentioned above since it occurs mainly in LREE deposits associated with alkaline or carbonatite rocks. Bastnäsite was first described by the Swedish chemist Wihelm Hisinger in 1838, who named it after the Bastnäs Mine near Riddarhyttan, Vastmanland, Sweden. The occurrences are known from carbonatites, alkali granites and syenites, pegmatites, hydrothermal deposits, skarns, fenites and other metasomatic rocks. Usually, most bastnäsites are bastnäsite-(Ce), and cerium (Ce) is by far the most common of the rare earth elements in this class of minerals. In addition, bastnäsite and monazite are the two largest and most preferred sources of LREE; however, bastnäsite is always the preferable choice over monazite because the high Th content of monazite presents a problem in LREE extraction. Moreover, bastnäsite ranks as first among the major LREE minerals (such as Al clays, xenotime, loparite and parasite) (Anton and Frances 2012). The Bayan Obo, Mianning–Dechang and Weishan deposits in China and Mountain Pass, California, USA are the best-known bastnäsite-bearing LREE deposits in the World (Yang *et al.* 2014a).

As a main ore mineral in LREE deposits, bastnäsite has the potential to record the primary geochemical and isotopic signature of the ore-forming process. Although bastnäsite is unstable in residual fluids, it is normally resistant to weathering processes; hence, it will normally remain unaltered when other minerals will be intensely weathered (Anton and Frances 2012). Additionally, bastnäsite has moderate Sr and low Rb mass fractions which make it suitable to obtain initial Sr isotope ratios that can then be applied to help decipher the petrogenesis and evolution of the LREE ore deposit. Furthermore, since the correction for *in situ* decay is small, the $^{87}Sr/^{86}Sr$ ratio can be considered as the initial Sr isotopic composition of the ore in which the bastnäsite crystallised (Yang *et al.* 2009a, 2014b). In addition, according to available geochemical data, bastnäsite also contains moderate U, Th and LREE contents (10% *m/m* Nd), as well as moderate Sr (> 200 μg g^{-1}), with low Rb (< 2 μg g^{-1}) and, hence, extremely low $^{87}Rb/^{86}Sr$ ratio (generally less than 0.001). These characteristics make this mineral a suitable candidate for U-Th-Pb geochronology and Sr-Nd analysis by laser sampling (Yang *et al.* 2009a, Sal'Nikova *et al.* 2010, Yang *et al.* 2014a, b).

Despite the frequent occurrence of bastnäsite in carbonatites and alkaline rocks, and its association with LREE deposits, few publications exist dealing with this mineral using La-Ba and U-Pb dating by traditional isotope dilution thermal ionisation mass spectrometry (ID-TIMS; Nakai *et al.* 1988, 1989, Sal'Nikova *et al.* 2010). In the present contribution, we report a comprehensive series of laser ablation *in situ* U-Th-Pb and Sr-Nd isotopic measurements in bastnäsite from various and typical LREE ore deposits around the world. Our aim is to identify suitable bastnäsite reference materials by using *in situ* U-Th-Pb and Sr-Nd isotopic measurement that can be used by the geochemical research community working with LREE ore deposits.

Analytical methods

Forty-seven bastnäsite samples were separated using a Frantz magnetic separator and were concentrated with heavy liquids. They were then selected by hand picking under a binocular microscope. All separated grains were embedded in epoxy, sectioned to expose their interiors, polished and mapped by optical microscopy and back-scattered electron imaging. Samples for solution Sr and Sm-Nd isotope analysis were determined directly by multi-collector inductively coupled plasma mass spectrometry (MC-ICP-MS), *in situ* trace element and U-Th-Pb age determination by LA-ICP-MS and Sr-Nd isotopic measurement by LA-MC-ICP-MS following the method of Yang *et al.* (2008, 2009b, 2011a, 2014a) and Liu *et al.* (2012), hence only a brief description is given below (Table 1). All analyses were conducted at the Institute of Geology and Geophysics, Chinese Academy of Sciences, Beijing.

Bastnäsite reference material

A well-characterised reference material (RM) is critical for *in situ* U-Th-Pb determination using ion or laser probe. There is no bastnäsite reference material for bastnäsite U-Th-Pb geochronology available. For this study, we used the bastnäsite reference material K-9 from the Karasug complex deposit, which is related to the carbonatites of the central Tuva area, Mongolia. The studied minerals were collected from supergene-altered haematite-bearing siderite carbonatites with baritocelestine, and come from the same set of bastnäsite crystals studied by Sal'Nikova *et al.* (2010).

The K-9 bastnäsite crystals are compositionally homogeneous (Figure 1a). Two bastnäsite microsamples consisting of two and three grains 250–500 mm in size were previously dated by Sal'Nikova *et al.* (2010) using the U-Pb method by ID-TIMS. The authors obtained a concordant age of 118 ± 1 Ma (MSWD = 0.05, probability = 0.82) (Figure 2a), which is in good agreement with a Sm-Nd age of 116 ± 8 Ma (bastnäsite) and 115 ± 7 Ma (fluorite) and a

Table 1.
Typical instrument parameters of U-Th-Pb dating of bastnäsite by LA-ICP-MS and its Sr-Nd isotopic analysis by LA-MC-ICP-MS

MC-ICP-MS cup configuration									
Faraday cups	L4	L3	L2	L1	Centre	H1	H2	H3	H4
Nominal mass	83	83.5	84	85	86	86.5	87	88	89
Sr^+			$^{84}Sr^+$		$^{86}Sr^+$		$^{87}Sr^+$	$^{88}Sr^+$	
$[Kr^+,Rb^+,HREE^{2+}]$	$^{83}Kr^+$,$^{166}Er^{2+}$	$^{167}Er^{2+}$	$^{84}Kr^+$,$^{168}Er^{2+}$,$^{168}Yb^{2+}$	$^{85}Rb^+$,$^{170}Er^{2+}$,$^{170}Yb^{2+}$	$^{86}Kr^+$,$^{172}Yb^{2+}$	$^{173}Yb^{2+}$	$^{87}Rb^+$,$^{174}Yb^{2+}$	$^{176}Yb^{2+}$	$^{89}Y^+$
Nominal mass	142	143	144	145	146	147	148	149	150
Nd^+	$^{142}Nd^+$	$^{143}Nd^+$	$^{144}Nd^+$	$^{145}Nd^+$	$^{146}Nd^+$		$^{148}Nd^+$		$^{150}Nd^+$
$[Ce^+,Sm^+]$	$^{142}Ce^+$		$^{147}Sm^+$			$^{147}Sm^+$	$^{148}Sm^+$	$^{149}Sm^+$	$^{150}Sm^+$

Instrumentations		
Mass spectrometers	Thermo Fisher Neptune MC-ICP-MS	Agilent 7500a Q-ICP-MS
RF forward power (W)	~ 1300	~ 1400
Interface cones	Nickel	Nickel
Integration times	0.262 s for laser Sr and Nd isotope 4.191 s for solution Sr or Nd isotopes	6 ms for Rb, Sr, Ba, Nb, Ta, Zr, Hf and REE, 15 ms for $^{204, 206, 208}Pb$, 30 ms for ^{207}Pb, 10 ms for ^{232}Th & ^{238}U
Background/baseline	30 s on-peak zero (OPZ)	20 s
Carrier gas (l min^{-1})	~ 0.75	~ 0.85
Laser ablation systems	Coherent Geolas Plus	Analyte G2
Laser system	ComPex 102, ArF excimer UV 193nm	ATLex 300si, ArF excimer UV 193nm
Ablation cell and volume	Standard circle low volume cell, volume *ca.* 4 cm^3	The commercial HeLEx dual-volume sample cell
Fluence	~ 4 J/cm^2 for Trace, U-Th-Pb dating, ~ 6 J cm^{-2} for Sr-Nd isotope	
Spot diameter	40 μm for Trace, U-Th-Pb dating, 16–32 μm for Nd isotope, 44–90 μm for Sr isotope	
Ablation duration	60 s for Trace, U-Th-Pb dating, 60 s for Sr or Nd isotope	
Sampling mode/repetition rate	Static spot ablation/~ 4–8 Hz	
Sample preparation	Conventional mineral separation, 1 inch resin mount	
Sample type/mineral	Bastnäsite, monazite and apatite	
Imaging	Transmissive light, reflected light and BSE imaging	
Data processing		
Gas blank	30 s on-peak zero subtracted	
Calibration strategy	In-house Tuva (K-9) bastnäsite was used as primary RM, LZ (1384) is used as a secondary RM for validation.	
Reference material information	Tuva (K-9) (Sal'Nikova *et al.* 2010) (ID-TIMS)	
Data processing package used/correction for LIEF	Glitter software for U-Th-Pb data processing and in-house spreadsheet for data normalisation of *in situ* Sr or Nd isotope, uncertainty propagation and age calculation. LIEF correction assumes reference material and samples behave identically.	
Mass discrimination	Tuva (K-9) used for initial mass bias correction with $^{207}Pb/^{206}Pb$ and $^{206}Pb/^{238}U$ additionally normalised to reference material.	
Common Pb correction	^{207}Pb common correction is applied to the $^{206}Pb/^{238}U$ and/or $^{208}Pb/^{232}Th$ age data by Isoplot software.	
Uncertainty level and propagation	Ages are quoted at 2*s* absolute, propagation is by quadratic addition. Reproducibility and age uncertainty of reference material and common Pb composition uncertainty are propagated where appropriate.	
Quality control/validation	$^{206}Pb/^{238}U$ age of LZ (1384) = 30 ± 1 Ma, $^{143}Nd/^{144}Nd$ of ZM (E) = 0.512758 ± 20 (2*s*), $^{87}Sr/^{86}Sr$ of LZ (1384) = 0.70620 ± 10 (2*s*), systematic uncertainty for propagation is 2% (2*s*).	

Rb-Sr age of 118 ± 9 Ma (muscovite) from carbonatites from the Karasug deposit, central Tuva (Sal'Nikova *et al.* 2010). The K-9 bastnäsite has U, Th and Pb contents of ~ 163, ~ 1161 and 12 μg g^{-1}, respectively, and a Th/U ratio of ~ 7 (Yang *et al.* 2014a). In this study, we used the K-9 bastnäsite as the primary U-Th-Pb reference material in the following sample measurements.

Major element determination

Major element compositions and back-scattered electron (BSE) observations were obtained using a JEOL-JAX8100 electron microprobe at a 15 kV accelerating potential and 12 nA beam current. Counting times were 20 s. Total iron is expressed as Fe_2O_3. The analytical uncertainties are within 2% for TiO_2 and CaO, but ~ 10–20% for other minor elements due to their low mass fractions.

In situ trace element and U-Th-Pb age determination

An Agilent 7500a Q-ICP-MS coupled to a 193 nm ArF excimer laser ablation system was used to determine trace element compositions and U-Pb ages. Helium was used as the carrier gas through the ablation cell and was mixed with argon downstream of the ablation cell (Table 1). Prior to analysis, the pulse/analogue (P/A) factor of the detector was calibrated using a standard tuning solution. The carrier and make-up gas flows were optimised to obtain maximum signal intensity for $^{238}U^+$, while keeping the ThO^+/Th^+ ratio below 0.5%. All LA-ICP-MS measurements were carried out using time-resolved analysis in fast, peak jumping mode. The dwell time for each isotope was set at 6 ms for Rb, Sr, Ba, Nb, Ta, Zr, Hf and REE, 10 ms for ^{232}Th, ^{238}U, 15 ms for ^{204}Pb, ^{206}Pb, ^{208}Pb and 30 ms for ^{207}Pb. A matrix-matched in-house reference material consisting of a crystal of K-9 bastnäsite was used to correct for U-Th-Pb fractionation and instrumental mass discrimination. Two K-9 and LZ1384 or MAD809 analyses were measured after every five unknown bastnäsite spots. The crater mode, rather than the raster mode, was adopted and the total ablated time took about 20 s for blank and 60 s for a single reference material or sample measurement.

Signals of ^{204}Pb, ^{206}Pb, ^{207}Pb, ^{208}Pb, ^{232}Th and ^{238}U were acquired for U-Th-Pb dating, whereas the ^{235}U signal was calculated from ^{238}U on the basis of the ratio $^{238}U/^{235}U = 137.818$. All measured $^{207}Pb/^{206}Pb$, $^{207}Pb/^{235}U$ and $^{206}Pb/^{238}U$ isotopic ratios of the K-9 reference material during sample analyses were regressed and corrected following the method of Sal'Nikova *et al.* (2010). Reference values of 0.04838 ($^{207}Pb/^{206}Pb$), 0.1232 ($^{207}Pb/^{235}U$), 0.01847 ($^{206}Pb/^{238}U$) and 0.005855 ($^{208}Pb/^{232}Th$) for K-9 bastnäsite were used in our work (Sal'Nikova *et al.* 2010), assuming a Th-Pb age equivalent to the U-Pb crystallisation age of 118 Ma. Uncertainties of the calibrated isotope ratios include those from the sample, reference material and deviations from the 'external' reference materials. The uncertainty was measured at *ca.* 2%. The U-Pb or Th-Pb ages, and weighted mean ages were calculated using the Isoplot/EX 3.23 software package (Ludwig 2003). Quantitative results for trace elements were obtained via the calibration of relative element sensitivities using NIST SRM 610 and normalisation of each analysis to ^{140}Ce as the internal standard element using Glitter software (Griffin *et al.* 2008). The Ce_2O_3 content in bastnäsite samples was determined by electron probe microanalysis as detailed in the previous section.

Accurate correction for laser-induced elemental fractionation and instrumental drift is an important consideration in U-Th-Pb dating of accessory minerals by LA-ICP-MS measurements. In this study, we used the matrix-matched in-house K-9 reference material to correct for U-Th-Pb elemental fractionation and variations in sensitivity during a measurement session. Another significant difficulty of U-Th-Pb dating of bastnäsite is the high common Pb content, which is incorporated in the mineral crystallisation phase. As noted by Chew *et al.* (2014), common Pb correction is typically undertaken using either concordia or isochron plots on a suite of co-genetic grains or, alternatively, on individual analyses using an appropriate choice of initial Pb isotopic composition (Williams 1998). In this study, the ^{207}Pb correction method was applied for common Pb correction assuming a Pb composition equivalent to Stacey and Kramers (1975), intercept age or $^{206}Pb/^{238}U$ weighted ages were calculated using Isoplot 3.23. Moreover, the intercepts of the regression line through the raw data on a Tera-Wasserburg plot provide an estimate of the $^{207}Pb/^{206}Pb$ ratio for the common Pb component (upper intercept) and the inferred crystallisation age (lower intercept) (Yang *et al.* 2009b, 2014a, Wu *et al.* 2010a, b, c). Similarly, considering the lower U content of most bastnäsites, we also conducted $^{208}Pb/^{232}Th$ age calculations after common ^{207}Pb correction (Ling *et al.* 2016).

In situ Sr isotopic measurement

A blank Neptune MC-ICP-MS coupled to a 193 nm ArF excimer laser ablation system was used to determine Sr isotopic compositions. A spot size of 44–90 μm was employed with a 6–8 Hz repetition rate and an energy

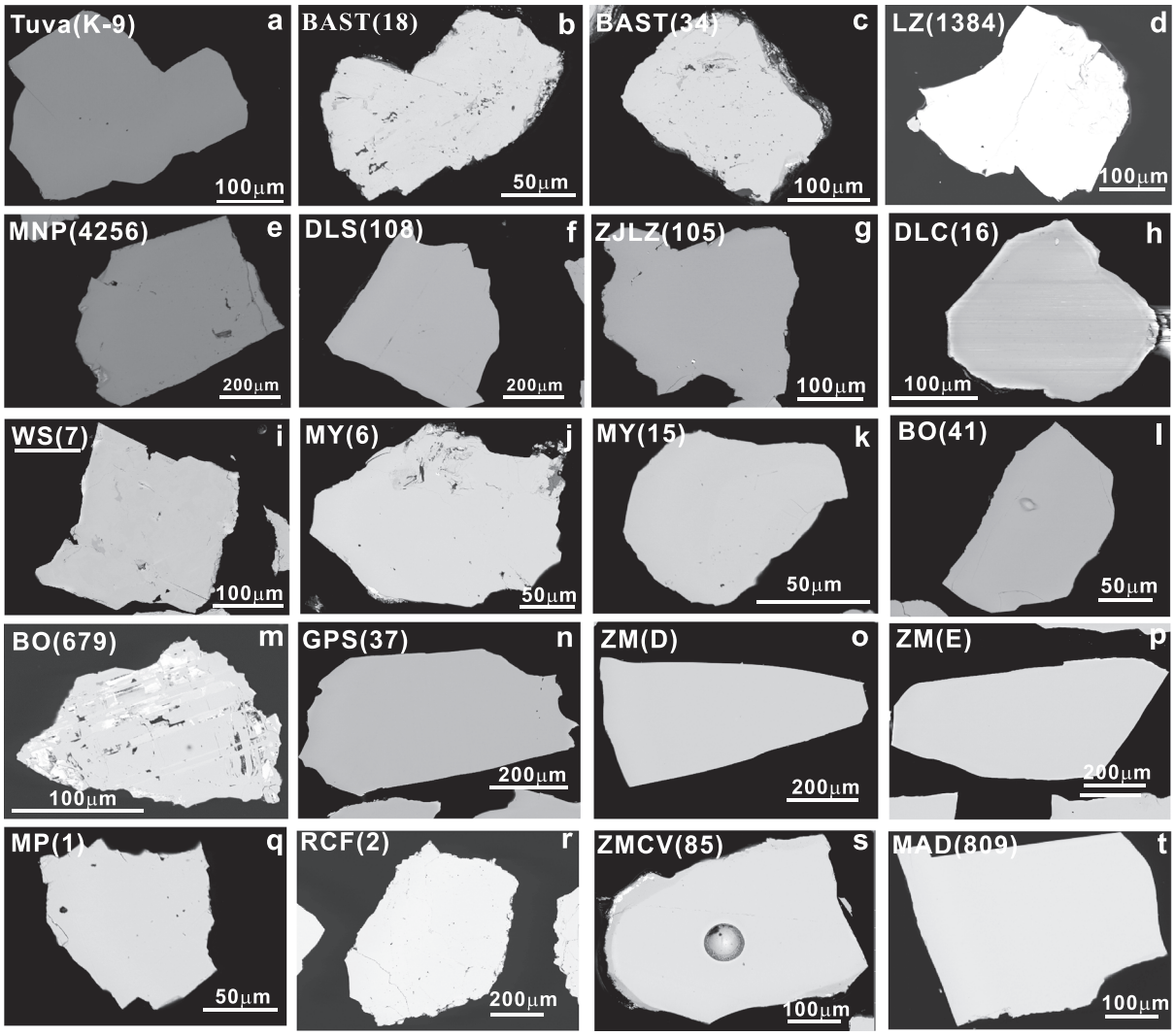

Figure 1. Back-scattered electron (BSE) images of typical bastnäsite samples investigated in this study. Most bastnäsite samples have clear images with homogenous compositions, indicating a high purity mineral. However, BO679 from Baya Obo shows a complex texture, indicating multi-stage mineralisation during formation.

density of ~ 6 J cm^{-2}, depending on the Sr mass fraction of the samples (Table 1). The Sr isotopic data were acquired by static multi-collection in low-resolution mode using nine Faraday collectors. Prior to laser analysis, the Neptune MC-ICP-MS was tuned using a standard solution to obtain maximum sensitivity. A typical data acquisition cycle consisted of a 20 s measurement of the Kr gas blank with the laser switched off, followed by 40 s of measurement with the laser ablating. Two LZ1384 or MAD809 in-house secondary bastnäsite reference materials were measured after every ten unknown samples for 'external' calibration (Yang *et al.* 2014b).

Data reduction was conducted offline, and the potential isobaric interferences were accounted for in the following order: Kr, Yb^{2+}, Er^{2+} and Rb. Firstly, the interference of ^{84}Kr and ^{86}Kr on ^{84}Sr and ^{86}Sr, respectively, was removed using the 30 s Kr gas baseline measurement. The isobaric interference correction of ^{84}Kr and ^{86}Kr on ^{84}Sr and ^{86}Sr was conducted using the natural Kr isotopic ratios ($^{83}Kr/^{84}Kr$ = 0.20175, $^{83}Kr/^{86}Kr$ = 0.66474; Christensen *et al.* 1995, Bizzarro *et al.* 2003). Secondly, the presence of $^{167}Er^{2+}$ and $^{173}Yb^{2+}$ at masses 83.5 and 86.5 was monitored based on the protocols of Ramos *et al* (2004). Using the isotopic abundances of Er and Yb (Chartier *et al.* 1999, Horstwood *et al.* 2008, Ling *et al.* 2016), the potential doubley-charged ion isobaric interference of $^{166}Er^{2+}$ (at *m/z* 83), $^{168}Er^{2+}$ (at *m/z* 84) and $^{170}Er^{2+}$ (at *m/z* 85) on $^{83}Kr^{+}$, $^{84}Sr^{+}$ and $^{85}Rb^{+}$, respectively, was evaluated and corrected by monitoring the interference-free $^{167}Er^{2+}$ (at *m/z* 83.5)

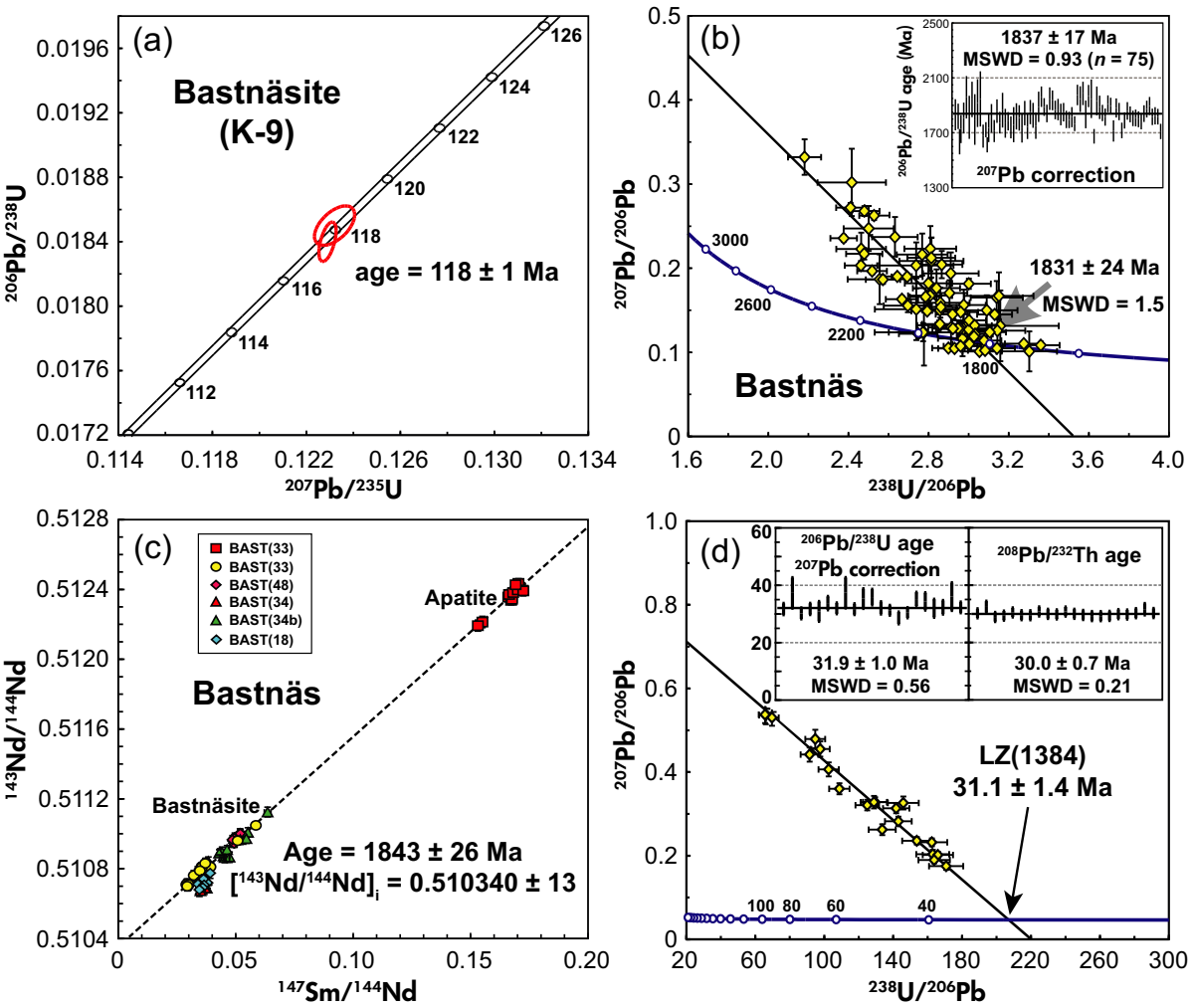

Figure 2. (a) Wetherill concordia plot showing results of U-Pb isotope measurements for bastnäsite K-9 by ID-TIMS. Ellipses represent 2*s*. Data are from Sal'Nikova *et al.* (2010). (b, c) Comparison of U-Pb and Sm-Nd ages derived from a Tera-Wasserburg concordia plot after common Pb correction (b) and a Sm-Nd isochron plot (c) of bastnäsite samples from Bastnäs Mines, Sweden. (d) Comparison of U-Pb (Tera-Wasserburg plot), $^{206}Pb/^{238}U$ and ^{208}Pb-^{232}Th ages after common Pb correction of LZ1384 bastnäsite from the Lizhuang REE deposit, Sichuan, China. Uncertainty bars for individual analyses are 1SE (in-run uncertainty) for age. MSWD: mean square of weighted deviates. [Colour figure can be viewed at wileyonlinelibrary.com]

signal intensity. Similarly, the potential doubley-charged ion isobaric interference of $^{170}Yb^{2+}$ (at *m/z* 85), $^{172}Yb^{2+}$ (at *m/z* 86), $^{174}Yb^{2+}$ (at *m/z* 87) and $^{176}Yb^{2+}$ (at *m/z* 88) on $^{85}Rb^{+}$, $^{86}Sr^{+}$, $^{87}Sr^{+}$ and $^{88}Sr^{+}$, respectively, was assessed and corrected for by monitoring the interference-free $^{173}Yb^{2+}$ (at *m/z* 86.5) signal intensity (Yang *et al.* 2014b). Thirdly, the natural ratio of $^{85}Rb/^{87}Rb$ (2.5926) was used to correct for isobaric interference of ^{87}Rb on ^{87}Sr by the exponential law, assuming that Rb has the same mass discrimination behaviour as Sr (Woodhead *et al.* 2005). It is observed that the obtained $^{87}Rb/^{87}Sr$ ratio is typically less than 0.001 during *in situ* bastnäsite Sr measurement, indicating that the radiogenic ^{87}Sr contribution is negligible (Yang *et al.* 2014b). In addition, our previous work demonstrated that Ca argides and dimers had an insignificant influence on Sr isotope analysis using a Neptune MC-ICP-MS (Yang *et al.* 2014b), a conclusion that is also strongly supported by other studies (Vroon *et al.* 2008). Therefore, interferences from Ca argides or dimers are not considered further in this work. Finally, the $^{87}Sr/^{86}Sr$ ratios were calculated and normalised from the interference-corrected $^{86}Sr/^{88}Sr$ ratio using an exponential law. The whole data reduction procedure was performed using an in-house Excel VBA (Visual Basic for Applications) macro program.

In situ Nd isotopic measurement

A Neptune MC-ICP-MS coupled to a 193 nm ArF excimer laser ablation system was used to determine Nd isotope ratios. Prior to laser analyses, the Neptune MC-ICP-MS was tuned and optimised for maximum sensitivity using a JNdi-1 standard solution. A laser spot size of 16–32 μm was employed with a 6–8 Hz repetition rate, depending on the Nd mass fraction of the samples. Each spot analysis consisted of approximately 60 s data acquisition with the laser fire on (Yang *et al.* 2008) (Table 1). Two measurements of the K-9 *in-house* reference material were undertaken after every ten unknowns. The LZ1384 or ZM (E) in-house secondary bastnäsite reference material was analysed in each measurement session and treated as an unknown sample during the data reduction procedure (Yang *et al.* 2014b, Ling *et al.* 2016).

In order to obtain accurate $^{147}Sm/^{144}Nd$ and $^{143}Nd/^{144}Nd$ bastnäsite data by LA-MC-ICP-MS, care must be taken to adequately correct for the contribution of the isobaric interference of ^{144}Sm on the ^{144}Nd signal. The Sm interference correction is complicated by the fact that the $^{146}Nd/^{144}Nd$ ratio, which is conventionally used to normalise the other Nd isotope ratios, is also affected by Sm interference. As a result, the mass bias correction of ^{144}Sm interference on ^{144}Nd cannot be applied directly from the measured $^{146}Nd/^{144}Nd$ ratio (Foster and Vance 2006, McFarlane and McCulloch 2007, 2008, Yang *et al.* 2008, 2009b, Wu *et al.* 2010a, b, c, Fisher *et al.* 2011, Mitchell *et al.* 2011). In this work, we have adopted the recently revised Sm isotopic abundances ($^{147}Sm/^{149}Sm$ = 1.08680 and $^{144}Sm/^{149}Sm$ = 0.22332) (Dubois *et al.* 1992, Isnard *et al.* 2005). Firstly, we used the measured $^{147}Sm/^{149}Sm$ ratio to calculate the Sm fractionation factor and the measured ^{147}Sm intensity by employing the natural $^{147}Sm/^{144}Sm$ ratio of 4.866559 (Isnard *et al.* 2005) to estimate the Sm interference on mass 144. Then, the interference-corrected $^{146}Nd/^{144}Nd$ ratio can be used to calculate the Nd fractionation factor. Finally, the $^{143}Nd/^{144}Nd$ and $^{145}Nd/^{144}Nd$ ratios were normalised using the exponential law. The $^{147}Sm/^{144}Nd$ ratio of unknown samples can also be calculated using the exponential law after correcting for isobaric interference of ^{144}Sm on ^{144}Nd as described above. The $^{147}Sm/^{144}Nd$ ratio was then 'externally' further calibrated against the $^{147}Sm/^{144}Nd$ ratio of a K-9 reference material during the measurement sessions (Yang *et al.* 2013). The raw data were exported offline, and the whole data reduction procedure was performed using an in-house Excel VBA (Visual Basic for Applications) macro program.

Strontium and Nd isotopic determination by the solution method

Chemical separation was undertaken by conventional ion-exchange techniques. Bastnäsite crystals were dissolved with a mixed ^{149}Sm-^{150}Nd spike in 2.5 ml concentrated Hcl, 0.2 ml HNO_3 and $HClO_4$ using 7 ml round-bottomed Savillex™ PTFE screw-top capsules placed in an oven for a week at 190 °C. Following complete dissolution and spike-sample homogenisation, each sample was evaporated to dryness at high temperature (fuming $HClO_4$) on a hot plate; then the mixture was treated with 6 mol l^{-1} HCl, evaporated to dryness and taken up in 3 mol l^{-1} HCl before chemical separation. The treatment with 6 mol l^{-1} HCl is necessary to completely convert fluorides into chlorides (Yang *et al.* 2011a). The first stage involved standard cation exchange chromatography for Rb and Sr purification. Following this, the Sr fraction was further purified by Sr-specific resin prior to mass spectrometric measurement (Yang *et al.* 2012). The REE eluted with 6 mol l^{-1} HCl was further purified using another Eichrom Ln resin (100–150 μm, 2 ml) with 0.25 mol l^{-1} HCl for Nd and 0.40 mol l^{-1} HCl for Sm (Yang *et al.* 2010b, 2011a).

Strontium and Sm-Nd isotopes were determined using a Neptune MC-ICP-MS. Procedural blanks were less than 100 pg Sr, and 50 pg for Sm and Nd. $^{87}Sr/^{86}Sr$ and $^{143}Nd/^{144}Nd$ ratios were normalised to $^{86}Sr/^{88}Sr$ = 0.1194 and $^{146}Nd/^{144}Nd$ = 0.7219 using the exponential law. During the period of data acquisition, analyses yielded results of $^{87}Sr/^{88}Sr$ = 0.710250 ± 11 (2*s*, *n* = 18) for NBS987 and $^{143}Nd/^{144}Nd$ = 0.512110 ± 12 (2*s*, *n* = 12) for Jndi-1. Additionally, USGS reference materials BCR-2 and BHVO-2 were also processed for Sr-Nd isotopes and gave ratios of 0.704997 ± 12 ($2s_m$) and 0.703474 ± 11 ($2s_m$) for $^{87}Sr/^{86}Sr$, 0.512635 ± 10 ($2s_m$) and 0.513000 ± 15 ($2s_m$) for $^{143}Nd/^{144}Nd$, respectively, which is identical, within uncertainty, to the recommended values of TIMS (Weis *et al.* 2005, 2006).

Method validation of *in situ* U-Th-Pb age and Sr-Nd isotopic analysis

To validate the reliability of our *in situ* U-Pb data, six bastnäsite samples collected from the Bastnäs Mine, Sweden, were analysed for *in situ* U-Pb age and Sm-Nd isotopic data. As presented in Figure 2b, all samples yielded an intercept U-Pb age of 1831 ± 24 Ma (2*s*, *n* = 75, 2*s* means 2SE of one sample by multiple analysis in one measurement session, the same mean in the following sections) without anchoring the upper common $^{207}Pb/^{206}Pb$ composition, in good agreement with the 1837 ± 17 Ma

(2*s*, *n* = 75) common ^{207}Pb correction age and also identical to the 1843 ± 26 Ma age of an *in situ* Sm-Nd isochron age within uncertainty (Figure 2c). The consistency between the *in situ* U-Pb and Sm-Nd age for the same samples indicates the robustness of our technique. Moreover, as shown in Figure 2d, the consistency of the U-Th-Pb age of LZ1384 (31.9 ± 1.0 Ma intercept age; 31.1 ± 1.4 Ma following common ^{207}Pb correction for $^{206}Pb/^{238}U$ age, 30.0 ± 0.7 Ma following common ^{207}Pb correction for $^{208}Pb/^{232}$ Th age) is also thought to demonstrate the reliability of our current protocol.

Similarly, to assess *in situ* Sr-Nd isotopic protocols, several bastnäsite samples (LZ1384, K-9, ZM (E) and MAD809) were repeatedly measured by solution and laser ablation methods during our method development. As summarised in Table 2, the $^{87}Sr/^{86}Sr$ ratio obtained by LA-MC-ICP-MS for the LZ1384 and MAD809 bastnäsites was 0.70623 ± 13 (2*s*, *n* = 22) and 70844 ± 7 (2*s*, *n* = 12), respectively, agreeing well with those data obtained by the solution method (0.70621 ± 2 ($2s_m$), 0.70619 ± 2 ($2s_m$) for LZ1384 and 0.70845 ± 3 ($2s_m$) for MAD809, respectively). Moreover, the Sr and Nd isotopic compositions of K-9 by laser sampling were 0.70570 ± 25 (2*s*, *n* = 12) for $^{87}Sr/^{86}Sr$ and 0.512780 ± 13 (2*s*, *n* = 45) for $^{143}Nd/^{144}Nd$, respectively, which are in good agreement with 0.70556 ± 2 ($2s_m$) and 0.70558 ± 2 ($2s_m$) of $^{87}Sr/^{86}Sr$, 0.512767 ± 4 (2*s*) and 0.512763 ± 4 (2*s*) of $^{143}Nd/^{144}Nd$ for bastnäsite of the same location using solution MC-ICP-MS and ID-TIMS (Sal'Nikova *et al.* 2010) (Table 2). Our solution results of 0.0338 and 0.0317 for $^{147}Sm/^{144}Nd$ and 0.512508 ± 10 ($2s_m$) and 0.512485 ± 9 ($2s_m$) for $^{143}Nd/^{144}Nd$ ratios for two individual grains of LZ1384 are identical to 0.0357 and 0.512512 ± 12 (2*s*, *n* = 15) within uncertainty by laser ablation. In summary, our obtained *in situ* Sr-Nd isotopic data by LA-MC-ICP-MS are also identical to those solution data by multiple analyses, indicating the feasibility of our method for *in situ* Sr-Nd isotopic measurement of bastnäsite (Table 2). Therefore, these bastnäsite samples were used for data monitoring during *in situ* laser ablation measurements of Sr and Nd isotopes.

Applications

In order to demonstrate the effectiveness and strength of our developed protocol, we measured natural bastnäsite samples from sixteen LREE ore deposits or alkali granite complexes around the world: Mianning-Dechang, Sichuan, Weishan, Shandong, Miaoya, Hubei, Bayan Obo, Inner Mongolia and Guposhan, Guangxi (China), Zagi Mountain (Pakistan), Bastnäs Mine (Sweden), Karasug Teva (Mongolia), Mountain Pass, California and Red Cloud Fluorite Mine, New Mexico (USA), Zomba-Malosa, Chilwa (Malawi), and Ambatofinandrahana (Madagascar). The results are compared with available published data. A detailed sample description is given in Appendix S1, and information about the different localities is summarised in Table 3.

The samples were investigated in detail, and typical BSE images are presented in Figure 1. Representative major and trace element compositions of bastnäsites from different samples are given in online supporting information Table S1, and the trace element variation diagram patterns are shown in Figure 3. The data obtained in this study by the laser ablation method allow comparisons of the trace element and isotopic composition of bastnäsite from various localities. The *in situ* U-Th-Pb ages and Sr-Nd isotopic data for the analysed bastnäsite, together with monazite or apatite from the samples are summarised in Table 4. As recommended by Horstwood *et al.* (2016) for LA-ICP-MS geochronology, the supporting information data are appended as Table S2 (*in situ* U-Th-Pb laser data), Table S3 (*in situ* Sr laser data) and Table S4 (*in situ* Sm-Nd laser data)).

China

Mianning-Dechang (Sichuan): The Mianning-Dechang (MNDC) REE belt, located in western Sichuan, China, includes one giant (Maoniuping, MNP), one large (Dalucao, DLC), one intermediate (Muluozhai, MLZ) and several small REE deposits (e.g., Lizhuang, LZ). The carbonatite-alkaline complexes consist of carbonatitic sills or dykes and associated alkaline syenite stocks. A few available radiometric dates define a metallogenic age of 10 to 40 Ma determined by the K-Ar-Ar method for biotite and muscovite, and U-Pb dating of zircon by SHRIMP (Xu *et al.* 2008, Xu et al. 2012, Hou *et al.* 2009, Tian *et al.* 2008, Liu *et al.* 2015).

Maoniuping: We obtained a $^{208}Pb/^{232}Th$ age of 26.9 ± 0.5 Ma (2*s*, *n* = 12) for bastnäsite sample MNP4256 (Figures 1e and 4a). These data are in good agreement, within uncertainty, with the 25.7 ± 0.2 Ma age (2*s*, *n* = 20) obtained by Ling *et al.* (2016) using SIMS. The other three bastnäsite samples (MNP1241, 1242 and 1243) yielded $^{208}Pb/^{232}Th$ ages of 25.7 ± 0.8 Ma (2*s*, *n* = 10), 26.0 ± 0.6 Ma (2*s*, *n* = 19) and 26.3 ± 0.7 Ma (2*s*, *n* = 12), respectively (Figure 4a, b). The $^{87}Sr/^{86}Sr$ ratios obtained by LA-MC-ICP-MS for these four bastnäsite samples (MNP4256, 1241, 1242 and 1243) are 0.70651 ± 6 (2*s*, *n* = 13), 0.70653 ± 9 (2*s*, *n* = 11), 0.70650 ± 6 (2*s*, *n* = 12) and 0.70614 ± 6 (2*s*, *n* = 12), respectively. The

Table 2.
Comparison of laser and solution Sr-Nd isotopic data of bastnäsite samples

Sample	Age (Ma)	$^{87}Rb/^{86}Sr$	$^{87}Sr/^{86}Sr$ (±2*s*)	I_{Sr}	Sm ($\mu g\ g^{-1}$)	Nd ($\mu g\ g^{-1}$)	$^{147}Sm/^{144}Nd$	$^{143}Nd/^{144}Nd$ (±2*s*)	$\varepsilon_{Nd(t)}$ (±2*s*)	Method
LZ (1384)	30	0.0018	0.70623 (13)	0.7062			0.0357	0.512512 (12)	-1.85 (0.23)	LA-MC-ICP-MS
			0.70621 (02)	0.7062	4139	73935	0.0338	0.512508 (10)	-1.91 (0.20)	Sol. MC-ICP-MS
			0.70619 (02)	0.7062	4153	79193	0.0317	0.512485 (09)	-2.35 (0.18)	Sol. MC-ICP-MS
ZM (E)	37						0.0652	0.512729 (07)	+2.39 (0.14)	LA-MC-ICP-MS
					17186	171574	0.0606	0.512756 (11)	+2.94 (0.21)	Sol. MC-ICP-MS
					18211	206777	0.0532	0.512760 (12)	+3.06 (0.23)	Sol. MC-ICP-MS
Tuva (K-9)	118	0.0019	0.70570 (25)	0.7057			0.0762	0.512780 (13)	+4.58 (0.25)	LA-MC-ICP-MS
			0.70556 (02)	0.7056	11130 [a]	87650 [a]	0.0768 [a]	0.512767 (04) [a]	+4.32 (0.08) [a]	Sol. MC-ICP-MS
			0.70558 (02)	0.7056	10470 [a]	84300 [a]	0.0751 [a]	0.512763 (04) [a]	+4.27 (0.08) [a]	Sol. MC-ICP-MS
MAD (809)	520	0.0005	0.70844 (07)	0.7084			0.0304	0.511309 (17)	-14.89 (0.34)	LA-MC-ICP-MS
			0.70845 (03)	0.7084						Sol. MC-ICP-MS

[a]Obtained by ID-TIMS (Sal'Nikova *et al.* 2010), others measured by solution or laser MC-ICP-MS in this study.

initial Sr isotope ratios range from 0.7061 to 0.7065 (Table 4), in good agreement with 0.7061–0.7066 for $^{87}Sr/^{86}Sr$ ratios by TIMS for calcite, barite and fluorite from the MNP LREE deposit (Hou *et al.* 2009). *In situ* Sm-Nd measurements in bastnäsite using laser ablation yielded $^{147}Sm/^{144}Nd$ and $^{143}Nd/^{144}Nd$ ratios of 0.0368 and 0.512426 ± 15 (2*s*, *n* = 15), 0.0381 and 0.512495 ± 12 (2*s*, *n* = 15), 0.0363 and 0.512489 ± 14 (2*s*, *n* = 15) and 0.0349 and 0.512495 ± 16 (2*s*, *n* = 15), respectively (Table 4), the corresponding $\varepsilon_{Nd(t)}$ values for these four samples are -3.60 ± 0.30 (2*s*), -2.26 ± 0.24 (2*s*), -2.37 ± 0.26 (2*s*) and -2.26 ± 0.30 (2*s*), respectively, which is almost identical to $^{143}Nd/^{144}Nd$ ratios obtained by TIMS from calcite and fluorite from the MNP LREE deposit (Hou *et al.* 2009). The initial Nd isotope data for these samples are consistent within analytical uncertainty.

Muluozhai: The Muluozhai (MLZ) LREE deposit consists of two small deposits: the Diaoloushan (DLS) and the Zhengjialiangzi (ZJLZ). As shown in Figures 4c–e, our nine DLS bastnäsite samples yielded a Th-Pb age of ~ 27 Ma. The different ages are consistent with each other within uncertainty. Recently, Ling *et al.* (2016) reported a SIMS Th-Pb bastnäsite age of 26.9 ± 0.2 Ma (2*s*, *n* = 20) and 26.7 ± 0.2 Ma (2*s*, *n* = 20), respectively. Our obtained *in situ* Sr and Sm-Nd data for the DLS LREE deposit samples are also in good agreement with each other (Table 4). The initial Sr isotope data are ~ 0.7071–0.7072, and the $\varepsilon_{Nd(t)}$ value ranges from -2.55 to -3.21. A 0.7066 value for $^{87}Sr/^{86}Sr$ ratios by TIMS for calcite from this LREE deposit was previously reported by Hou *et al.* (2009). At the same time, the three bastnäsite samples from Zhengjialiangzi (ZJLZ) also yielded a Th-Pb age of ~ 28 Ma (Figure 4f). Moreover,

Table 3.
Summary information for bastnäsite samples investigated in this study

Sample (numbers/names)	Location	Host rock
MNP (4256, 1241, 1242, 1243)	Maoniuping, Sichuan, China	Pegmatitic vein in alkaline syenite
DLS (108, 105, 106a, 106b, 110, 114, 115, 119, 121)	Diaoloushan, Sichuan, China	Pegmatitic vein in alkaline syenite
ZJLZ (103a, 103b, 105)	Zhengjialiangzi, Sichuan, China	Pegmatitic vein in alkaline syenite
LZ (122, 1381, 1382,1383a, 1383b, 1384)	Lizhuang, Sichuan, China	Pegmatitic vein in alkaline syenite
DLC (16, 43)	Dalucao, Sichuan, China	Pegmatitic vein in alkaline syenite
WS (7, 29, 9)	Weishan, Shandong, China	Pegmatitic vein in alkaline syenite
MY (6, 15)	Miaoya, Hubei, China	Carbonatite
BO (41, 138, 679)	Bayan Obo, Inner Mongolia, China	Carbonatite
GPS (37)	Guposhan, Guangxi, China	Granite
ZM (B, D, E)	Zagi Mountain, Pakistan	Aplite vein in alkaline granite
BAST (18, 34, 34b, 33, 48)	Bastnäs Mine, Sweden	Metavolcanics
Tuva (K-9)	Tuva, Mongolia	Carbonatite
MP (1)	Mountain Pass, California, USA	Carbonatite
RCF (2)	Red Cloud Fluorite Mine, New Mexico, USA	Fluorite-cemented hydrothermal breccias
ZMCV (85)	Zomba-Malosa, Chilwa, Malawi	Pegmatitic vein in alkaline granite
MAD (809)	Madagascar	Alkaline to peralkaline complex

the Sr and Nd isotopic compositions are also identical to those of the nine DLS samples.

Lizhuang: The obtained $^{208}Pb/^{232}Th$ ages for sample LZ122 (29.5 ± 0.6 Ma; 2*s*, *n* = 18) (Figure 4g) are in good agreement, within uncertainty, with the 28.4 ± 0.2 Ma age (2*s*, *n* = 20) obtained by SIMS (Ling *et al.* 2016). The other five bastnäsite samples LZ1381, 1382, 1383a, 1383b and 1384 yielded $^{208}Pb/^{232}Th$ ages of 28.2 ± 0.6 Ma (2*s*, *n* = 19), 28.9 ± 0.7 Ma (2*s*, *n* = 19), 28.7 ± 0.7 Ma (2*s*, *n* = 18), 30.1 ± 0.8 Ma (2*s*, *n* = 18), 30.0 ± 0.7 Ma (2*s*, *n* = 21), respectively (Figure 4g, h). The $^{87}Sr/^{86}Sr$ ratios obtained by LA-MC-ICP-MS for the six bastnäsite samples are 0.70628 ± 4 (2*s*, *n* = 24), 0.70642 ± 10 (2*s*, *n* = 9), 0.70637 ± 8 (2*s*, *n* = 10), 0.70650 ± 12 (2*s*, *n* = 10), 0.70641 ± 9 (2*s*, *n* = 10) and 0.70623 ± 13 (2*s*, *n* = 22), respectively (Table 4). The initial Sr isotope ratios range from 0.7062 to 0.7064, which is almost identical to 0.7063 and 0.7069 for $^{87}Sr/^{86}Sr$ ratios by TIMS for calcite from the same REE deposit (Hou *et al.* 2009).

The *in situ* bastnäsite Sm-Nd, using laser ablation, yielded $^{147}Sm/^{144}Nd$ and $^{143}Nd/^{144}Nd$ ratios of 0.0388 and 0.512450 ± 11 (2*s*, *n* = 22), 0.0360 and 0.512503 ± 9 (2*s*, *n* = 12), 0.0392 and 0.512500 ± 9 (2*s*, *n* = 15), 0.0344 and 0.512500 ± 12 (2*s*, *n* = 15), 0.0339 and 0.512505 ± 10 (2*s*, *n* = 15) and 0.0357 and 0.512512 ± 12 (2*s*, *n* = 15), respectively (Table 4). The corresponding $\varepsilon_{Nd(t)}$ values for these samples are -3.06 ± 0.20 (2*s*), -2.02 ± 0.18 (2*s*), -2.10 ± 0.18 (2*s*), -2.07 ± 0.23 (2*s*), -1.97 ± 0.19 (2*s*) and -1.85 ± 0.23 (2*s*), respectively (Table 4). The initial Nd isotope data for the six samples are consistent within analytical uncertainty and also agree well with those data from calcite by TIMS (Hou *et al.* 2009). Therefore, we consider that the age of this deposit is ~ 29 Ma, indicating a narrow range in the mineralisation age by direct determination of bastnäsite.

Dalucao: Our obtained $^{208}Pb/^{232}Th$ ages for samples DLC16 and DLC43 are 13.2 ± 0.6 Ma (2*s*, *n* = 8) and 13.4 ± 0.6 Ma (2*s*, *n* = 8) (Figure 4i), which are in good agreement with ages obtained by Ling *et al.* (2016) of 11.9 ± 0.2 (2*s*, *n* = 12) Ma and 11.8 ± 0.2 Ma (2*s*, *n* = 20), within uncertainty, by using the SIMS method. The $^{87}Sr/^{86}Sr$ ratios obtained by LA-MC-ICP-MS for these two samples are 0.70809 ± 9 (2*s*, *n* = 12) and 0.70818 ± 17 (2*s*, *n* = 12), respectively (Table 4). The initial Sr isotope ratios range from 0.7081 to 0.7082, which is higher than those for the other three REE deposits in MNDC, Sichuan. The *in situ* Sm-Nd data by using laser ablation yielded $^{147}Sm/^{144}Nd$ and $^{143}Nd/^{144}Nd$ ratios of 0.0274 and 0.512387 ± 13 (2*s*, *n* = 10), and 0.0343 and 0.512392 ± 12 (2*s*, *n* = 10), respectively. The corresponding $\varepsilon_{Nd(t)}$ values for these two samples are -4.62 ± 0.25 (2*s*) and -4.54 ± 0.23 (2*s*), respectively. The initial Nd isotope values for these two samples are consistent with each other within analytical uncertainty.

Weishan, Shandong: As shown in Figure 5a, our three bastnäsite samples yielded ages of 121.2 ± 1.0 Ma (WS7, 2*s*, *n* = 14), 123.8 ± 0.7 Ma (WS29, 2*s*, *n* = 20) and 121.2 ± 1.1 Ma (WS9, 2*s*, *n* = 14), respectively, which are

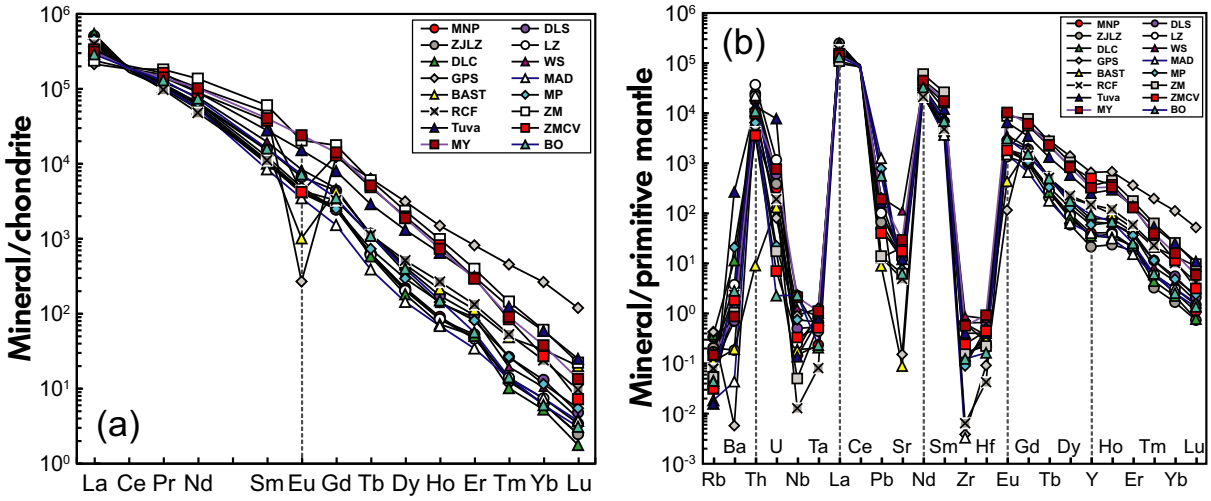

Figure 3. (a) Chondrite-normalised REE distribution patterns and (b) mantle-normalised patterns of bastnäsite samples analysed in this study. Normalisation values for both primitive mantle and chondrite are from McDonough and Sun (1995). Abbreviations: MNP, Maoniuping; DLS, Diaoloushan; ZJLZ, Zhengjialiangzi; LZ, Lizhuang; DLC, Dalucao; WS, Weishan; MY, Miaoya. [Colour figure can be viewed at wileyonlinelibrary.com]

in good agreement within uncertainties and are also identical to the 119.5 ± 1.7 Ma (2*s*, *n* = 6) Ma age of a muscovite Rb-Sr isochron and slightly older than a ~ 110 Ma muscovite K-Ar isochron age reported by Tian *et al.* (2002). The K-Ar age reported by Tian *et al.* (2002) for the host rock is ~ 140 Ma. The *in situ* Sr isotopes for the three samples yielded values of 0.70740 ± 2 (2*s*, *n* = 10), 0.70748 ± 4 (2*s*, *n* = 10) and 0.70727 ± 11 (2*s*, *n* = 13) (Table 4), respectively, and the corresponding initial Sr values are 0.7074, 0.7075 and 0.7073, respectively, indicating a similar genetic evolution or rock chemistry. Additionally, the values for *in situ* Sm-Nd isotope are 0.512092 ± 11 (2*s*, *n* = 12), 0.512074 ± 12 (2*s*, *n* = 13) and 0.512070 ± 11 (2*s*, *n* = 30), respectively, and the corresponding $\varepsilon_{Nd(t)}$ values are -8.48 ± 0.20 (2*s*), -8.66 ± 0.22 (2*s*) and -8.77 ± 0.21 (2*s*), respectively. As for the Rb-Sr system, the results of the Sm-Nd isotopic system indicate a relatively narrow age of mineralisation and the same genetic evolution or rock chemistry. The results of *in situ* Sr-Nd isotopic composition of the bastnäsite samples indicate that the source of the REE deposit is the enriched mantle.

Miaoya, Hubei: As illustrated in Figure 5b, our two bastnäsite samples yielded Th-Pb ages of 196.3 ± 2.8 Ma (MY6, 2*s*, *n* = 22) and 211.1 ± 4.1 Ma (MY15, 2*s*, *n* = 12), respectively. Our two monazite samples from the same locality yielded 229.8 ± 5.0 Ma (MY2, 2*s*, *n* = 14) and 232.1 ± 3.6 Ma (MY14, 2*s*, *n* = 18), respectively, which is similar to the 233.6 ± 1.7 Ma age of monazite from the same location dated by SHRIMP (Xu *et al.* 2014). Additionally, the MY15 bastnäsite for *in situ* Sr isotopes yielded 0.70358 ± 4 (2*s*, *n* = 14) (Table 4). The corresponding initial Sr ratio is 0.7036, which is identical to TIMS values reported by Xu *et al.* (2014) for whole rock and apatite from the same location. As shown in Table 4, the results of *in situ* Sm-Nd isotope data for bastnäsites and monazites are both in good agreement within their respective uncertainties.

Bayan Obo, Inner Mongolia: As presented in Figure 5c, the bastnäsite sample BO41 yielded a weighted mean $^{208}Pb/^{232}Th$ age of 274.2 ± 3.3 Ma (2*s*, *n* = 22), which represents the time of REE mineralisation. In addition, the two bastnäsite samples BO138 and BO679 yielded an extremely wide range of $^{208}Pb/^{232}Th$ ages from 320 Ma to 440 Ma (BO138) and from 240 Ma to 1360 Ma (BO679), which indicates a long period of REE mineralisation. The results of *in situ* Sr isotopes range from 0.71038 ± 37 (BO138, 2*s*, *n* = 12) to 0.70974 ± 15 (BO679, 2*s*, *n* = 15) (Table 4) with initial Sr values of 0.7104 and 0.7097, respectively. Moreover, the *in situ* Sm-Nd isotope values are 0.511454 ± 12 (2*s*, *n* = 11), 0.511277 ± 11 (2*s*, *n* = 10) and 0.511387 ± 16 (2*s*, *n* = 10), which yielded a reference Sm-Nd isochron of *ca.* 1400 Ma (Table 4).

During the last 20 years, several radiometric dating techniques have been applied to date the mineralisation of the Bayan Obo deposit, resulting in significantly different ages. These include the U-Th-Pb, Sm-Nd, Rb-Sr, K-Ar, Ar-Ar, Re-Os and La-Ba methods (Fan *et al.* 2014, 2016 and references therein). Based on previous La-Ba, Th-Pb and Sm-Nd isotopic data for the main REE ore minerals (monazite and bastnäsite), the oldest age of mineralisation is about 1300–1400 Ma (Nakai *et al.* 1989, Ren *et al.* 1994, Zhang *et al.* 2003, Yang *et al.* 2011b, 2011a) whereas the youngest is about 200–300 Ma, although according to Wang *et al.* (1994) and Chao *et al.* (1997) there are multiple phases of mineralisation.

Guposhan, Guangxi: The GPS37 bastnäsite collected from the Guposhan granite, Guangxi Province, southern China, yielded a Th-Pb age of 161.4 ± 1.5 Ma (2*s*, *n* = 13) of (Figure 6a), which is in good agreement with a U-Pb age of ~ 163 Ma for three zircons dated by LA-ICP-MS (Gu *et al.* 2006). These results demonstrate that the entire Guposhan granite formed at the same time. As shown in Table 4 and Figure 7, this conclusion is also supported by similar Nd isotopic values for bastnäsite by laser ablation in the present study ($\varepsilon_{Nd(t)}$ = -2.89 ± 0.17) (2*s*, *n* = 12) and a whole-rock granite sample by ID-TIMS ($\varepsilon_{Nd(t)}$ = -4.06 ± 0.84 (2*s*, *n* = 8)) (Gu *et al.* 2006).

Pakistan

Our three gem-quality bastnäsite specimens (0.5 × 1.5 × 2.0 cm) come from Zagi Mountain (Pechawar), located in the north-western Frontier Province, Pakistan. The ZM B, D and E bastnäsites yielded 37.8 ± 1.2 Ma (2*s*, *n* = 24), 37.4 ± 1.1 Ma (2*s*, *n* = 24) and 36.2 ± 1.6 Ma (2*s*, *n* = 16) (Figure 6b), respectively, which are slightly younger than ages reported for the host granitic rock: 41 Ma (K-Ar, riebeckite), 40 ± 5 Ma (Ar-Ar, riebeckite), 43.5 ± 5 Ma (Ar-Ar, riebeckite) and 42 ± 4 Ma (Ar-Ar, biotite) (Kempe 1973, Maluski and Matte 1984). The results for *in situ* Sm-Nd isotopes are 0.512737 ± 10 (2*s*, *n* = 12), 0.512725 ± 9 (2*s*, *n* = 12) and 0.512729 ± 7 (2*s*, *n* = 12), respectively, and the corresponding $\varepsilon_{Nd(t)}$ mean values are + 2.50 ± 0.20 (2*s*), +2.25 ± 0.18 (2*s*) and + 2.39 ± 0.14 (2*s*), respectively, indicating a relatively narrow range for the mineralisation age and a similar genetic evolution or rock chemistry (Table 4). Furthermore, the gem-quality bastnäsite is also a potential reference material candidate for *in situ* Nd isotope analysis by laser ablation.

Table 4.
Compilation of Sr, Sm-Nd isotopic data and corresponding initial Sr and Nd of bastnäsites investigated in this study

Sample	Age (Ma)	$^{87}Rb/^{86}Sr$	$^{87}Sr/^{86}Sr$ (±2*s*)	I_{Sr}	$^{147}Sm/^{144}Nd$	$^{143}Nd/^{144}Nd$ (±2*s*)	$\varepsilon_{Nd(t)}$ (±2*s*)
MNP 4256	26	0.0013	0.70651 (06)	0.7065	0.0368	0.512426 (15)	-3.60 (0.30)
MNP 1241	26	0.0012	0.70653 (09)	0.7065	0.0381	0.512495 (12)	-2.26 (0.24)
MNP 1242	26	0.0011	0.70650 (06)	0.7065	0.0363	0.512489 (14)	-2.37 (0.26)
MNP 1243	26	0.0007	0.70614 (06)	0.7061	0.0349	0.512495 (16)	-2.26 (0.30)
DLS 108	27	0.0019	0.70710 (07)	0.7071	0.0438	0.512445 (10)	-3.21 (0.20)
DLS 105	27	0.0018	0.70723 (13)	0.7072	0.0386	0.512455 (08)	-3.01 (0.16)
DLS 106a	27	0.0027	0.70714 (07)	0.7071	0.0378	0.512453 (10)	-3.04 (0.19)
DLS 106b	27	0.0045	0.70710 (05)	0.7071	0.0360	0.512457 (11)	-2.95 (0.22)
DLS 110	27	0.0035	0.70724 (08)	0.7072	0.0412	0.512452 (08)	-3.08 (0.15)
DLS 114	27	0.0010	0.70720 (09)	0.7072	0.0451	0.512479 (07)	-2.55 (0.13)
DLS 115	27	0.0019	0.70706 (11)	0.7071	0.0433	0.512472 (05)	-2.69 (0.11)
DLS 119	27	0.0010	0.70720 (11)	0.7072	0.0505	0.512473 (09)	-2.69 (0.18)
DLS 121	27	0.0012	0.70712 (15)	0.7071	0.0403	0.512463 (09)	-2.86 (0.19)
ZJLZ 103a	27	0.0005	0.70708 (10)	0.7071	0.0271	0.512441 (09)	-3.27 (0.18)
ZJLZ 103b	27	0.0016	0.70698 (09)	0.7070	0.0264	0.512440 (17)	-3.28 (0.32)
ZJLZ 105	27	0.0027	0.70717 (07)	0.7072	0.0280	0.512452 (10)	-3.04 (0.19)
LZ 122	30	0.0005	0.70628 (04)	0.7063	0.0388	0.512450 (11)	-3.06 (0.20)
LZ 1381	30	0.0010	0.70642 (10)	0.7064	0.0360	0.512503 (09)	-2.02 (0.18)
LZ 1382	30	0.0011	0.70637 (08)	0.7064	0.0392	0.512500 (09)	-2.10 (0.18)
LZ 1383a	30	0.0013	0.70650 (12)	0.7065	0.0344	0.512500 (12)	-2.07 (0.23)
LZ 1383b	30	0.0009	0.70641 (09)	0.7064	0.0339	0.512505 (10)	-1.97 (0.19)
LZ 1384	30	0.0018	0.70623 (13)	0.7062	0.0357	0.512512 (12)	-1.85 (0.23)
DLC 16	13	0.0038	0.70809 (09)	0.7081	0.0274	0.512387 (13)	-4.62 (0.25)
DLC 43	13	0.0008	0.70818 (17)	0.7082	0.0343	0.512392 (12)	-4.54 (0.23)
WS 7	120	0.0001	0.70740 (02)	0.7074	0.0548	0.512092 (11)	-8.48 (0.20)
WS 29	120	0.0002	0.70748 (04)	0.7075	0.0431	0.512074 (12)	-8.66 (0.22)
WS 9	120	0.0001	0.70727 (11)	0.7073	0.0455	0.512070 (11)	-8.77 (0.21)
MY 2 [a]	230				0.0747	0.512428 (14)	-0.52 (0.28)
MY 6	230				0.0749	0.512427 (17)	-0.54 (0.33)
MY 14 [a]	230				0.0603	0.512410 (11)	-0.45 (0.20)
MY 15	230	0.0004	0.70358 (04)	0.7036	0.0722	0.512429 (12)	-0.42 (0.23)
BO 41	274				0.0531	0.511454 (12)	-18.08 (0.23)
BO 138	370	0.0003	0.71038 (37)	0.7104	0.0353	0.511277 (11)	-18.93 (0.22)
BO 679		0.0014	0.70974 (15)	0.7097	0.0489	0.511387 (16)	
GPS 37	161				0.0878	0.512376 (08)	-2.89 (0.17)
ZM B	37				0.0787	0.512737 (10)	+2.50 (0.20)
ZM D	37				0.0805	0.512725 (09)	+2.25 (0.18)
ZM E	37				0.0652	0.512729 (07)	+2.39 (0.14)
BAST 18	1840				0.0358	0.510718 (15)	+0.53 (0.24)
BAST 34	1840				0.0365	0.510707 (15)	+0.17 (0.25)
BAST 34b	1840				0.0373	0.510813 (21)	+2.06 (0.21)
BAST 33	1840				0.0360	0.510794 (57)	+1.99 (0.18)
BAST 33b	1840				0.1668	0.512359 (40)	+1.63 (0.26)
BAST 48	1840				0.0501	0.510972 (12)	+2.12 (0.14)
Tuva K-9	118	0.0019	0.70570 (25)	0.7057	0.0762	0.512780 (13)	+4.58 (0.25)
MP 1	1400	0.0003	0.70456 (08)	0.7045	0.0349	0.511025 (15)	-2.44 (0.24)
RCF 2	29	0.0016	0.70719 (13)	0.7072	0.0463	0.512475 (13)	-2.61 (0.25)
ZMCV 85	114	0.0010	0.70617 (21)	0.7062	0.0638	0.512656 (16)	+2.29 (0.18)
MAD 809	520	0.0005	0.70844 (07)	0.7084	0.0304	0.511309 (17)	-14.89 (0.34)

[a] Monazite and [b] Apatite, others bastnäsite.

USA

Mountain Pass, California: As illustrated in Figure 6c, twenty-three analyses of bastnäsite sample MP1 yielded a mean Th-Pb age of 1422 ± 20 Ma (2*s*, *n* = 23). In addition, the $^{87}Sr/^{86}Sr$ and $^{143}Nd/^{144}Nd$ ratios are 0.70456 ± 8 (2*s*, *n* = 12) and 0.511025 ± 15 (2*s*, *n* = 12), respectively (Table 4). The corresponding initial Sr

isotope ratio is 0.7045, and the mean $\varepsilon_{Nd(t)}$ is -2.44 ± 0.24 (2*s*). Our results support a similar source for the carbonatitic fluids and suggest that the age of bastnäsite mineralisation is associated with the carbonatite intrusion, dated at ~ 1400 Ma (Dewitt *et al.* 1987). Recently, Jacob *et al.* (2016) reported a crystallisation age for titanite and zircon from Mountain Pass ranging from 1429 ± 10 to 1385 ± 18 Ma, increasing the age range of the ultrapotassic rocks in the complex by ~ 20 Ma. Meanwhile, the Th-Pb monazite crystallisation age of carbonatite samples is inferred to be ~ 1405 to 1395 Ma and ~ 1380 to 1370 Ma (Jacob *et al.* 2016), which is attributed to variable but minor radiogenic Pb loss. The $\varepsilon_{Nd(t)}$ for bastnäsite sample MP-P0913-SQ1 is -3.2 ± 0.3 (2*s*, *n* = 25) which is consistent with our result from sample MP1. Therefore, we consider that this famous LREE deposit formed at ~ 1400 Ma.

Red Cloud Fluorite Mine, New Mexico: As shown in Figure 6d, our eighteen Th-Pb analyses yielded a mean age of 29.3 ± 0.5 Ma (2*s*, *n* = 18) that is in good agreement with a K-Ar age of 29.9 Ma reported by Perhac (1970) for an orthoclase from a trachyte/syenite (Gallinas Mountains). The $^{87}Sr/^{86}Sr$ and $^{143}Nd/^{144}Nd$ ratios are 0.70719 ± 13 (2*s*, *n* = 12) and 0.512475 ± 13 (2*s*, *n* = 12), respectively (Table 4), whereas the corresponding initial Sr ratio is 0.7072 and the mean $\varepsilon_{Nd(t)}$ is -2.61 ± 0.25 (2*s*).

Malawi

As shown in Figure 6e, our twenty-three analyses of sample ZMCV485 yielded a mean Th-Pb age of 114.5 ± 2.0 Ma (2*s*), whereas the $^{87}Sr/^{86}Sr$ and $^{143}Nd/^{144}Nd$ ratios are 0.70617 ± 21 (2*s*, *n* = 12) and 0.512656 ± 16 (2*s*, *n* = 12), respectively (Table 4). The corresponding initial Sr ratio is 0.7062, and the mean $\varepsilon_{Nd(t)}$ is +2.29 ± 0.18 (2*s*). The age is in good agreement with the 113 ± 4 Ma age of emplacement of the Zomba-Malosa pear-shaped pluton reported by Eby *et al.* (1995). Recently, the emplacement age of pegmatites was well constrained by a single-zircon Pb–Pb evaporation age of 123 ± 4 Ma,

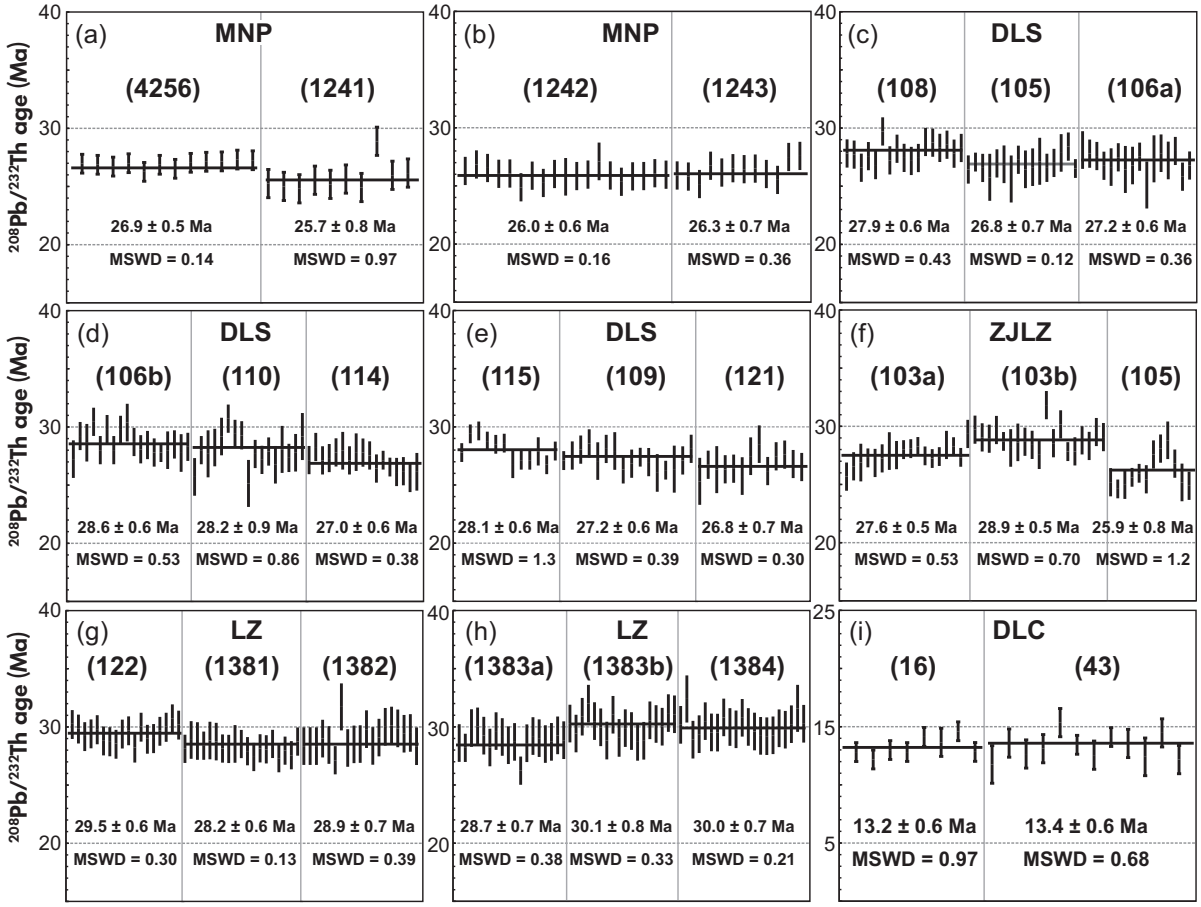

Figure 4. Th-Pb ages obtained by LA-ICP-MS for bastnäsites from the MNP, DLS, ZJLZ, LZ and DLC, MNDC LREE deposits, Sichuan province, China. Uncertainty bars for individual analyses are 1SE (in-run uncertainties). Abbreviations as in Figure 3. [Colour figure can be viewed at wileyonlinelibrary.com]

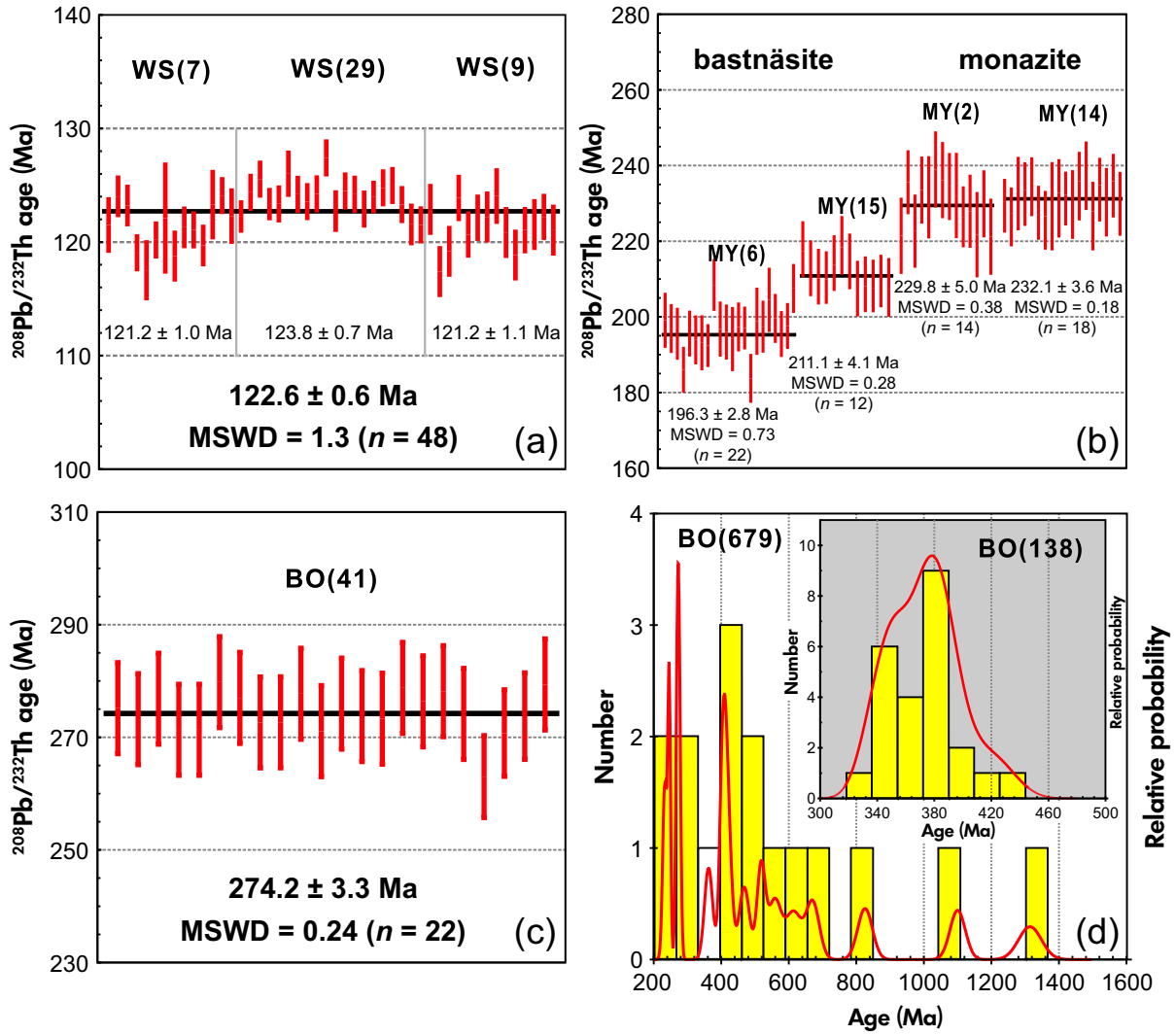

Figure 5. Th-Pb ages of bastnäsites from Weishan, Shandong, Miaoya, Hubei and Bayan Obo, Inner Mongolia, China. [Colour figure can be viewed at wileyonlinelibrary.com]

a zircon U–Pb SIMS age of 117 ± 1 Ma, a zircon U-Pb LA-ICP-MS age of 119.3 ± 2.1 Ma (zircon I) and 118.0 ± 1.2 Ma (zircon II) (Soman *et al.* 2010). These data indicate the reliability of the present technique.

Madagascar

Fourteen analyses of sample MAD809 yielded a mean Th-Pb age of 519.9 ± 4.5 Ma (2*s*) (Figure 6f). The Sr and Nd isotopic compositions are 0.70844 ± 7 (2*s*, *n* = 12) for $^{87}Sr/^{86}Sr$ and 0.511309 ± 17 (2*s*, *n* = 12) for $^{143}Nd/^{144}Nd$, respectively, the corresponding initial Sr ratio is 0.7084, and the mean $\varepsilon_{Nd(t)}$ is -14.89 ± 0.34 (2*s*) (Table 4). As noted by Rasoamalala *et al.* (2014), the bastnäsite and monazite deposits of the Ambatofinandrahana region of Madagascar are closely associated with an alkaline to peralkaline complex of Pan-African age (~ 540–570 Ma) (Liu *et al.* 2012).

Discussion

Bastnäsite as a U-Th-Pb geochronometer

The potential of bastnäsite as a U-Th-Pb geochronometer has not been properly investigated. In the present study, we show that bastnäsite has U and Th mass fractions of 1–200 μg g^{-1} and 300–4000 μg g^{-1} (Table S1), which makes it possible to precisely measure the U-Th-Pb isotopic composition by either traditional TIMS or *in situ* (laser ablation or ion probe) techniques. However, several factors have to be taken into account before using this ore mineral for radiometric dating.

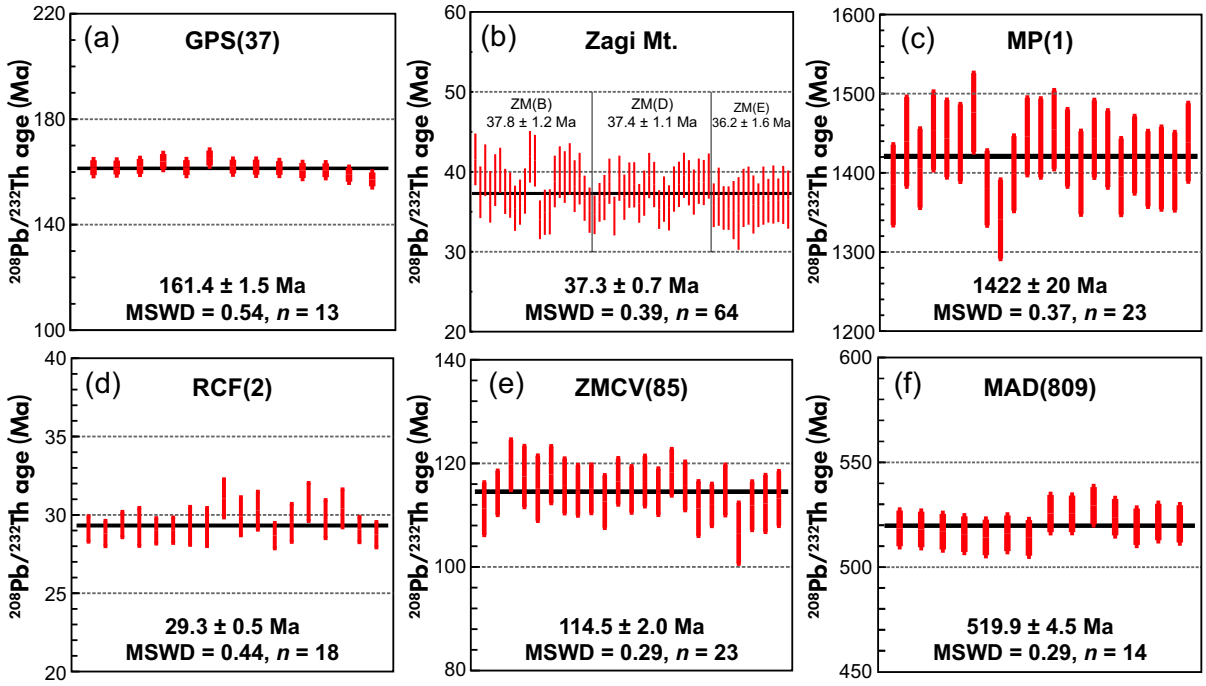

Figure 6. Th-Pb ages of bastnäsites from Guposhan (Guangxi, China), Zagi Mountain (Pakistan), Mountain Pass (California, USA), Red Cloud Fluorite Mine (New Mexico, USA), Zomba-Malosa (Chilwa, Malawi) and Ambatofinandrahana (Madagascar). [Colour figure can be viewed at wileyonlinelibrary.com]

Bastnäsite is easily altered and replaced by secondary zircon, apatite, monazite and other minerals. Some petrographic observations indicate that this mineral is susceptible to alteration during the late stage evolution of agpaitic magmas or thermal fluid activity (Williams-Jones *et al.* 2000). In our study, we observed that some bastnäsite samples display multi-stage alteration (BO679 from Bayan Obo). Consequently, *in situ* measurement techniques are preferable for U-Th-Pb isotopic determination.

Another problem relates to the U-Pb closure temperature of the mineral. To fully understand the U-Pb closure temperature of bastnäsite, a theoretical calculation is illustrated in Figure 8 where The kinetic porosity model of Zhao and Zheng (2007) is applied to the calculation of diffusion coefficients. The diffusion coefficients and closure temperatures of bastnäsite and monazite are thus compared. As shown in Figure 8, it is clear that small bastnäsite grains (radius *ca.* < 100 μm) have fast Pb diffusion rates and low closure temperatures. However, for larger grains the closure temperatures of monazite and bastnäsite are almost identical (Figure 8b). Therefore, it is readily understandable that the Th-Pb ages of bastnäsite are younger than that of monazite from the Miaoya Mine (Figures 1j, k and 5b).

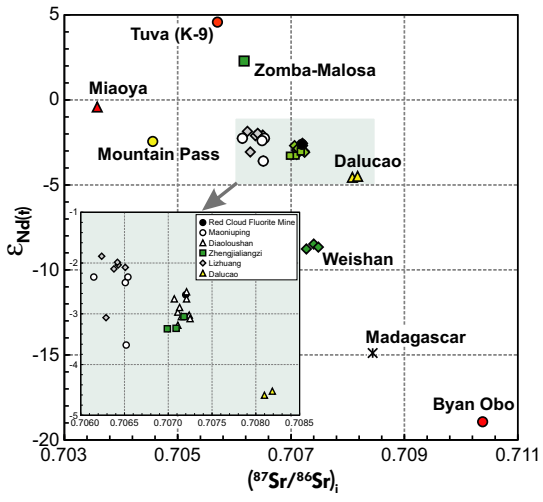

Figure 7. Initial $^{87}Sr/^{86}Sr$ and Nd isotopic compositions of bastnäsites investigated in this study. [Colour figure can be viewed at wileyonlinelibrary.com]

The U-Pb decay system, with two independent decay chains ($^{206}Pb/^{238}U$, $^{207}Pb/^{235}U$), offers an internal check on a closed system. This is the main advantage of the U-Pb system over the Th-Pb system ($^{208}Pb/^{232}Th$). However, although the $^{206}Pb/^{238}U$ vs. $^{208}Pb/^{232}Th$ age after ^{207}Pb

correction for bastnäsite samples from MNDC (e.g., LZ1384) is similar within uncertainties, the Th-Pb age has a better precision than the U-Pb age (Figure 2d). Moreover, other investigations of bastnäsite samples around the world also support this observation. As shown in Figure 9a, except for the Bastnäs and Tuva (K-9) samples, the remaining bastnäsite samples are characterised by much higher Th than U contents with Th/U ratios between 100 and 10000. The U contents of most bastnäsites are less than 10 μg g^{-1} except for samples MNDC and Tuva (K-9). Except for Bastnäs, Red CFM and Tuva (K-9), the f_{206} (common ^{206}Pb in proportion to total ^{206}Pb) of nearly all samples ranges from 10% to 100% and the f_{208} (common ^{208}Pb in proportion to total ^{208}Pb) is less than 20%, in which the f_{208} for most of these is lower than 10% (Figure 9b). Therefore, considerably higher radiogenic ^{208}Pb and considerably lower f_{208} give the Th-Pb system an overwhelming advantage over the U-Pb system for most bastnäsites.

Furthermore, the intermediate daughter isotope ^{230}Th will decay with a half-life of ~ 7500 a in the ^{238}U-^{206}Pb decay chain. The younger bastnaesite grains (e.g., LZ1384) with a very high Th/U ratio (between 100 and 10000) will incorporate excess ^{230}Th during crystallisation (Figure 2c). This excess ^{230}Th will completely decay into ^{206}Pb, which is not the daughter isotope of ^{238}U within the mineral (Scharer 1984). This is why the $^{206}Pb/^{238}U$ age after ^{207}Pb correction can be a bit older than the $^{208}Pb/^{232}Th$ age although they are similar within analytical uncertainty (Figure 2c). Hence, the excess radiogenic ^{206}Pb makes the U-Pb method more complex for young bastnaesite grains with high Th/U ratios (Ling *et al.* 2016). A similar situation is also observed for many other Th-rich accessory minerals such as monazite, allanite and perovskite. Despite the difficulties due to the excess or deficit of radiogenic ^{206}Pb, this problem does not exist for the Th-Pb system because each of the intermediate nuclei of the ^{232}Th-^{208}Pb decay chain has a very short half-life.

Potential of bastnäsite for *in situ* Sr-Nd isotopic measurement

Our previous work (Yang *et al.* 2009b, 2014b) demonstrated that a Sr mass fraction of ~ 500 μg g^{-1} in bastnäsite grains is enough to produce an absolute

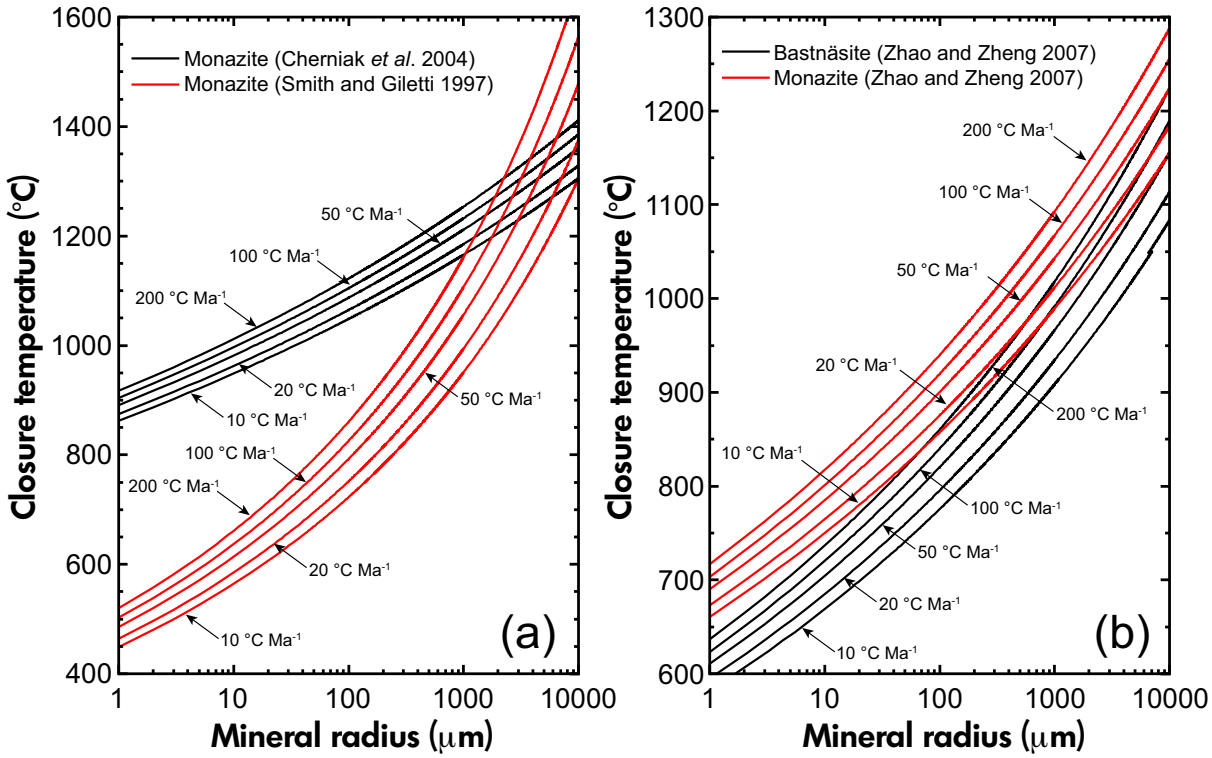

Figure 8. Theoretical calculation of Pb closure temperature of bastnäsite and monazite based on the methods of Smith and Giletti (1997), Cherniak *et al.* (2004) and Zhao and Zheng (2007). Note that bastnäsite has a Pb closure temperature of ~ 750–800 °C for a grain size of 100 μm at cooling rates of 10–200 °C Ma^{-1}. The diffusion coefficients of bastnäsite and monazite are from Zhao and Zheng (2007). [Colour figure can be viewed at wileyonlinelibrary.com]

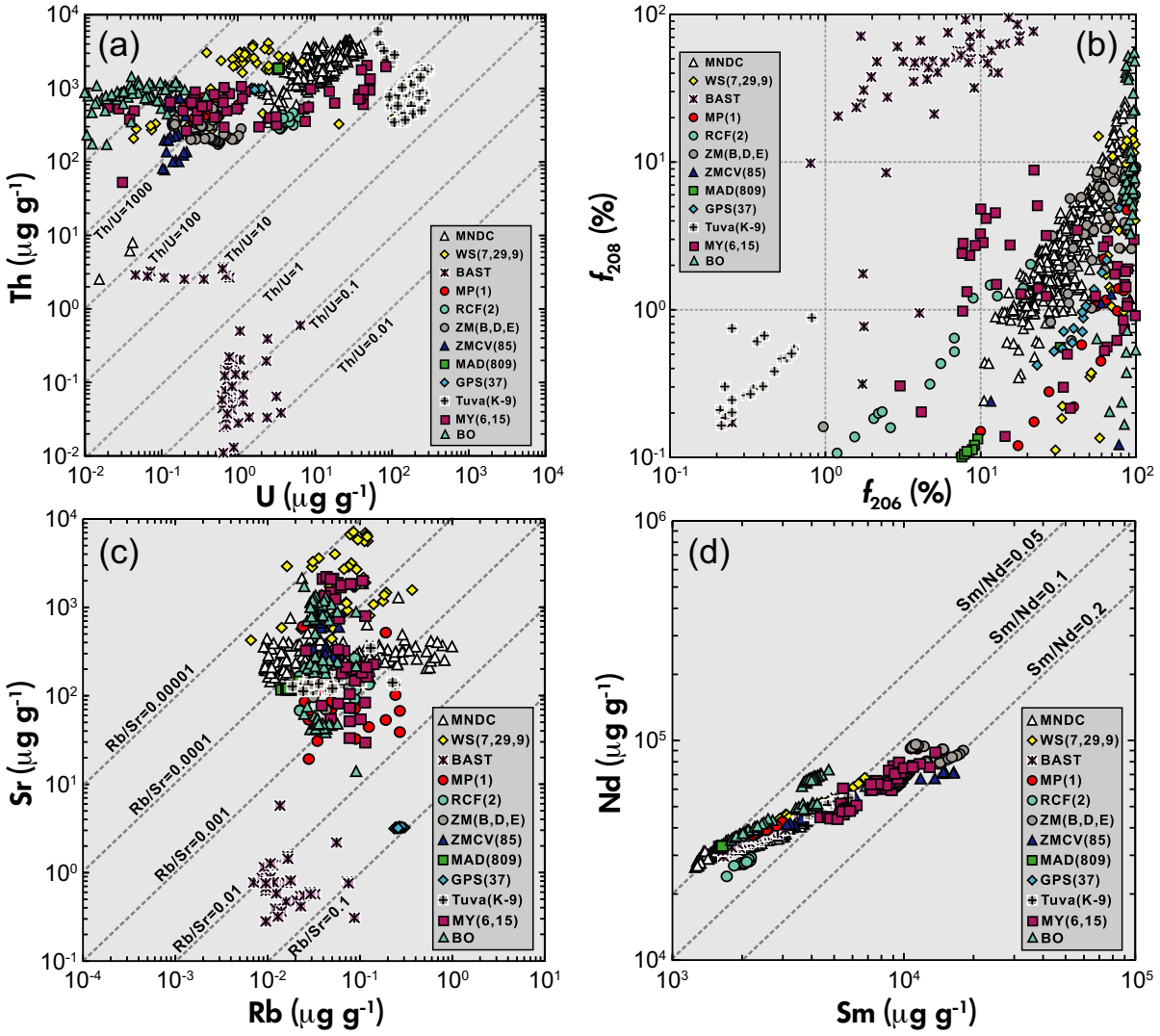

Figure 9. (a, b) Comparison between U and Th elemental mass fraction and between the f_{206} and f_{208} values as well as the percentage of common ^{206}Pb and ^{208}Pb in total ^{206}Pb and ^{208}Pb, respectively, of bastnäsites analysed in this study. The plot shows that most bastnäsites, except for Bastnäs Mine bastnäsite, have much lower f_{208} than f_{206} values. (c, d) Variations of Rb-Sr and Sm-Nd in the bastnäsite samples. [Colour figure can be viewed at wileyonlinelibrary.com]

precision of ± 0.0001 for the $^{87}Sr/^{86}Sr$ ratio when using a large laser spot size (100–160 μm). The extremely low Rb mass fraction (and hence very low Rb/Sr ratios) of bastnäsite mean that isobaric interference of ^{87}Rb on ^{87}Sr is usually insignificant and can easily be accounted for (Yang *et al.* 2011c) (Figure 9c). As most bastnäsites yield moderate Sr mass fractions, there is usually sufficient Sr for *in situ* Sr isotopic measurement, except for some from the Bastnäs Mine, Zagi Mountain and Guposhan localities (Table 4).

As shown in Figure 9d, bastnäsite grains with low Sm/Nd ratios (0.05–0.2) are ideal for *in situ* Sm-Nd isotopic measurement by laser sampling. As summarised in Table 2, the results obtained by laser (e.g., Zagi E, LZ1384, K-9, MAD809) are identical to solution data. This demonstrates the feasibility of our *in situ* Sm-Nd technique. Combined with their age and trace element, we can calculate the corresponding $\varepsilon_{Nd}(t)$ values (Table 4). In summary, the data presented in this study demonstrate that reliable Sr and Nd isotopic compositions can be obtained by LA-MC-ICP-MS for the majority of natural bastnäsite samples.

Bastnäsite RM for *in situ* U-Th-Pb dating and/or Sr-Nd isotopic measurement

Reference materials are essential for *in situ* analysis and are usually a prerequisite for precise analysis (e.g., zircon, apatite, monazite, titanite, etc.) (Wu *et al.* 2006, Liu *et al.* 2012).

An ideal reference material for *in situ* U-Th-Pb dating and/or Sr-Nd isotopic analysis of bastnäsite must meet the following criteria: (a) homogeneity in trace element content both within and between individual grains; (b) low Rb and reasonable Sr and Nd contents; (c) moderate U and Th mass fraction with low common Pb; (d) a well constrained crystallization age (e.g., U-Th-Pb age); (e) be available in sufficient quantity for the scientific community. Up to the present, there have been few available bastnäsite reference materials except for K-9.

As shown in Figures 9a, b, the Th/U ratio of K-9 is usually less than 10, which means excess ^{206}Pb from ^{230}Th has an insignificant effect on the $^{206}Pb/^{238}U$ age. Additionally, as shown in the diagram of the f_{206} vs. f_{208} (both in the range of 0.2–0.8%), the effect of common ^{206}Pb and ^{208}Pb on U-Th-Pb dating for LA-ICP-MS is almost negligible. Based on the results of the present study, we suggest that K-9 bastnäsite is a good candidate as a reference material for U-Th-Pb dating and *in situ* Sr-Nd isotope measurement (Table 2). Although K-9 has a relatively young age, it has a homogenous composition and comes in good gem-quality size. Moreover, samples LZ1384 and ZM E, although with relatively young age, can also be considered as a good secondary reference material for both *in situ* U-Th-Pb dating and/or Sr-Nd measurements. In addition, MAD809 with an age of ~ 520 Ma and negligible common ^{208}Pb is also a potential candidate as a reference material for Th-Pb age and *in situ* Sr-Nd measurement.

Conclusions

We demonstrate the capability and applicability of bastnäsite for U-Th-Pb geochronology and Sr-Nd isotopic measurement using *in situ* laser ablation measurement. Laser ablation can yield reasonable U-Th-Pb ages for the bastnäsite group of minerals as they have high Th and moderate U contents. However, a common Pb correction is necessary if reliable results are to be expected. Moreover, our diverse investigation indicates that a Th-Pb age is preferable over the U-Pb age because of the relatively higher Th than U content in most bastnäsites. Bastnäsite usually contains moderate Sr and high Nd content, coupled with low Rb/Sr and Sm/Nd ratios and laser ablation can yield reliable Sr and Nd isotopic data. Therefore, *in situ* analysis is preferable for the determination of age and isotopic composition. As an important ore mineral, the minerals of the bastnäsite group can be considered a promising and significant geochronological tool suitable for research on carbonatites, alkaline rocks and related LREE deposits.

Acknowledgements

This work was financially supported by the Chinese State Key Research and Development Programme (2016YFE0203000) and the Natural Science Foundation of China (Grants 41525012, 41273021, and 41703057). YRA acknowledges support from the Deutsche Forschungsgemeinschaft (DFG) grant RO 4174/3-1. We are very grateful to Matt Horstwood, Nick Roberts, David Chew and an anonymous reviewer for their critical and insightful comments on the initial draft, which significantly improved this manuscript. We are indebted to the following bastnäsite sample providers (A. Guastoni (ZMCV485), G.A. Davis (Mountain Pass), U.B. Anderson and Ulf Hålenius (Bastnäs Mine), Gunnar Färber Mineralien (Mountain Pass, Zagi Mt. E & RCF), E.B. Sal'Nikova (K-9), Tony Nikischer (Mountain Pass), S. Cisneros (Zagi Mt. B & D), Zhu-Ming Yang (GPS37, BO679 and MAD809)). We also thank the editor for his patience in handling this manuscript. We are willing to distribute these bastnäsite reference materials (K-9, LZ1384, Zagi Mt., MAD809, etc.) to other colleagues upon request.

References

Allen M.S. and Foord E.E. (1991)
Geological, geochemical, and isotopic characteristics of the Lincoln County porphyry belt, N.M.: Implications for regional tectonics and mineral deposits. **New Mexico Geological Society Fall Field Conference Guidebook**, **42**, 97–115.

Anczkiewicz R., Oberli F., Burg J.P., Villa I.M., Günther D. and Meir M. (2001)
Timing of normal faulting along the Indus Suture in Pakistan Himalaya and a case of major $^{231}Pa/^{235}U$ initial disequilibrium in zircon. **Earth and Planetary Science Letters**, **191**, 101–114.

Anglin C.D., Jonasson I.R. and Franklin J.M. (1996)
Sm-Nd dating of scheelite and tourmaline: Implications for the genesis of Archaean gold deposit, Val d'Or, Canada. **Economic Geology**, **91**, 1372–1382.

Anton R.C. and Frances W. (2012)
Rare earth elements: Minerals, mines, magnets (and more). **Elements**, **8**, 330–340.

Bizzarro M., Simonetti A., Stevenson R.K. and Kurszlaukis S. (2003)
In situ $^{87}Sr/^{86}Sr$ investigation of igneous apatites and carbonates using laser-ablation MC-ICP-MS. **Geochimica et Cosmochimica Acta**, **67**, 289–302.

Campbell L.S., Compston W., Sircombe K.N. and Wilkinson C.C. (2014)
Zircon from the East Ore body of the Bayan Obo Fe-Nb-REE deposit, China, and SHRIMP ages for carbonatite-related magmatism and REE mineralization events. **Contributions to Mineralogy and Petrology**, **168**, 1041–1065.

Castor S.B. (2008)
The Mountain Pass rare-earth carbonatite and associated ultrapotassic rocks, California. **The Canadian Mineralogist**, **46**, 779–806.

references

Castor S.B. and Nason G.W. (2004)
Mountain Pass rare earth deposit, California. In: Castor S.B., Papke K.G. and Meeuwig R.O. (eds), Proceedings of the 39th Forum on the geology of industrial minerals. Nevada Bureau of Mines and Geology, Special Publication, 33, 68–81.

Chao E.C.T., Back J.M., Minkin J.A., Tatsumoto M., Wang J., Conrad J.E., MaKee E.H., Hou Z. and Meng Q.S. (1997)
The sedimentary carbonate-hosted giant Bayan Obo REE-Fe-Nb ore deposit of Inner Mongolia, China: A cornerstone example for giant polymetallic ore deposits of hydrothermal original. United States Geological Survey Bulletin, 2143, 1–65.

Chartier F., Aubert M., Salmon M., Tabarant M. and Tran B.H. (1999)
Determination of erbium in nuclear fuels by isotope dilution thermal ionization mass spectrometry and glow discharge mass spectrometry. Journal of Analytical Atomic Spectrometry, 14, 1461–1465.

Che X.D., Wu F.Y., Wang R.C., Gerdes A., Ji W.Q., Zhao Z.H., Yang J.H. and Zhu Z.Y. (2015)
In-situ U-Pb isotopic dating of columbite-tantalite by LA-ICP-MS. Ore Geology Reviews, 65, 979–1465.

Cherniak D.J., Watson E.B., Grove M. and Harrison T.M. (2004)
Pb diffusion in monazite: A combined RBS/SIMS study. Geochimica et Cosmochimica Acta, 68, 829–840.

Chew D.M., Petrus J.A. and Kamber B.S. (2014)
U-Pb LA-ICP-MS dating accessory mineral standard with variable common Pb. Chemical Geology, 363, 185–199.

Christensen J.N., Halliday A.N., Lee D.C. and Hall C.M. (1995)
In situ Sr isotopic analysis by laser ablation. Earth and Planetary Science Letters, 136, 79–85.

DeWitt E., Kwak L.M. and Zartman R.E. (1987)
U-Th-Pb and $^{40}Ar/^{39}Ar$ dating of the Mountain Pass carbonatite and alkali igneous rocks, S.E. California. Geological Society of America, Abstracts with Programs, 19, 642.

Dubois J.C., Retali G. and Cesario J. (1992)
Isotopic analysis of rare earth elements by total vaporization of samples in thermal ionization mass spectrometry. International Journal of Mass Spectrometry, 120, 163–177.

Eby G.N., Roden-Tice M., Krueger H.L., Ewing W., Faxon E.H. and Woolley A.R. (1995)
Geochronology and cooling history of the northern part of the Chilwa alkaline province, Malawi. Journal of African Earth Science, 20, 275–288.

Fan H.R., Hu F.F., Yang K.F., Pirajno F., Liu X. and Wang K.Y. (2014)
Integrated U-Pb and Sm-Nd geochronology for a REE-rich carbonatite dyke at the giant Bayan Obo REE deposit, Northern China. Ore Geology Reviews, 63, 510–59.

Fan H.R., Yang K.F., Hu F.F., Liu S.S. and Wang K.Y. (2016)
The giant Bayan Obo REE-Nb-Fe deposit, China: Controversy and ore genesis. Geoscience Frontiers, 7, 335–344.

Fisher C.M., McFarlane C.R.M., Hanchar J.M., Schmitz M.D., Sylvester P.J., Lam R.L. and Henry P. (2011)
Sm-Nd isotope systematics by laser ablation-multicollector-inductively coupled plasma-mass spectrometry: Methods and potential natural and synthetic reference materials. Chemical Geology, 284, 1–20.

Foster G.L. and Vance D. (2006)
In situ Nd isotopic analysis of geological materials by laser ablation MC-ICP-MS. Journal of Analytical Atomic Spectrometry, 21, 288–296.

Griffin W.L., Powell W.J., Pearson N.J. and O'Reilly S.Y. (2008)
GLITTER: Data reduction software for laser ablation ICP-MS. In: Sylvester P. (ed.), Laser ablation-ICP-MS in the Earth sciences: Current practices and outstanding issues. Mineralogical Association Canada Short Course, 40, 308–311.

Gu S.Y., Hua R.M. and Qi H.W. (2006)
Study on zircon LA-ICP-MS U-Pb dating and Sr-Nd isotope of the Guposhan granite in Guangxi. Acta Geologica Sinica, 80, 543–553. (in Chinese with English abstract)

Guastoni A., Nestola F. and Giaretta A. (2009)
Mineral chemistry and alteration of rare earth element (REE) carbonates from alkaline pegmatites of Mount Malosa, Malawi. American Mineralogist, 94, 1216–1222.

Gulson B.L. and Jones M.T. (1992)
Cassiterite: Potential for direct dating of mineral deposits and a precise age for the Bushveld Complex granites. Geology, 20, 355–358.

Hisinger W. (1838)
Analyser av några svenska mineralier.2. Basiskt fluor-cerium från Bastnäs. Kungl. Vetenskaps-Akademiens Handlingar, 187, 1–9.

Holtstam D. and Andersson U.B. (2007)
REE mineralogy of the bastnäs-type deposits, south-central Sweden. The Canadian Mineralogist, 45, 1073–1114.

Horstwood M.S.A., Evans J.A. and Montgomery J. (2008)
Determination of Sr isotopes in calcium phosphates using laser ablation inductively coupled plasma-mass spectrometry and their application to archaeological tooth enamel. Geochimica et Cosmochimica Acta, 72, 5659–5674.

Horstwood M.S.A., Košler J., Gehrels G., Jackson S.E., McLean N.M., Paton C., Pearson N., Sircombe K., Sylvester P., Vermeesch P., Bowring J.F., Condon D.J. and Schoene B. (2016)
Community-derived standards for LA-ICP-MS U-(Th)-Pb geochronology – Uncertainty propagation, age interpretation and data reporting. Geostandards and Geoanalytical Research, 40, 311–332.

references

Hou Z., Tian S.H., Xie Y.L., Yang Z.S., Yuan Z.X., Yin S.P., Yi L.S., Fei H.C., Zou T.R., Bai G. and Li X.Y. (2009)
The Himalayan Mianning-Dechang REE belt associated with carbonatite-alkaline complexes, eastern Indo-Asian collision zone, SW China. **Ore Geology Reviews, 36**, 65–89.

Isnard H., Brennetot R., Caussignac C., Caussignac N. and Chartier F. (2005)
Investigations for determination of Gd and Sm isotopic compositions in spent nuclear fuels samples by MC-ICP-MS. **International Journal of Mass Spectrometry, 246**, 66–73.

Jacob E.P., John M.C., Graham A.H. and Jade S.L. (2016)
Petrochronological constraints on the origin of the Mountain Pass ultrapotassic and carbonatite intrusive suite, California. **Journal of Petrology, 57**, 1555–1598.

Kempe D.R.C. (1973)
The petrology of the Warsak alkaline granites, Pakistan, and their relationship to other alkaline rocks of the region. **Geological Magazine, 110**, 385–495.

Khattak N.U., Akram M., Ullah K., Qureshi A.A. and Qureshi I.E. (2004)
Recognition of emplacement time of Jambil carbonatites from NW Pakistan: Constraints from fission-track dating of apatite using age standard approach. **Geology Bulletin Union Peshawar, 37**, 127–138.

Khattak N.U., Qureshi A.A., Akram M., Ullah A., Azhar M. and Khan M.A. (2005)
Unroofing history of the Jambil and Jawar carbonatite complexes from NW Pakistan: Constraints from fission-track dating of apatite. **Journal of Asian Earth Sciences, 25**, 643–652.

Khattak N.U., Akram M., Khan M.A. and Khan H.A. (2008)
Emplacement time of the Loe-Shilman carbonatite from NW Pakistan: Constraints from fission-track dating. **Radiation Measurements, 43**, S313–S318.

Kynicky J., Smith M.P. and Xu C. (2012)
Diversity of rare earth deposits: The key example of China. **Elements, 8**, 361–367.

Lan T.G., Fan H.R., Hu F.F., Yang K.F. and Wang Y. (2011)
Genesis of the Weishan REE deposit, Shandong Province: Evidence from Rb-Sr isochron age, LA-MC-ICP-MS Nd isotopic composition and fluid inclusions. **Geochimica (Beijing), 40**, 428–442. (in Chinese with English abstract)

Le Bas M.J., Mian I. and Rex D.C. (1987)
Age and nature of carbonatite emplacement in north Pakistan. **Geologische Rundschau, 76**, 317–323.

Lin J., Liu Y.S., Yang Y.H. and Hu Z.C. (2016)
Calibration and correction of LA-ICP-MS and LA-MC-ICP-MS analyses for element contents and isotopic ratios. **Solid Earth Sciences, 1**, 5–27.

Ling X.X., Li Q.L., Liu Y.Yang and Y.H., Liu Y., Tang G.Q. and Li, X.H. (2016)
In situ SIMS Th-Pb dating of bastnäsite: Constraint on the mineralization time of the Himalayan Mianning-Dechang rare earth element deposits. **Journal of Analytical Atomic Spectrometry, 31**, 1680–1687.

Liu Y. and Hou Z.Q. (2017)
A synthesis of mineralization styles with an integrated genetic model of carbonatite-syenite-hosted REE deposits in the Cenozoic Mianning-Dechang REE metallogenic belt, the eastern Tibetan Plateau, southwestern China. **Journal of Asian Earth Sciences, 137**, 35–79.

Liu Z.C., Wu F.Y., Yang Y.H., Yang J.H. and Wilde S.A. (2012)
Neodymium isotopic compositions of the standard monazites used in U-Th-Pb geochronology. **Chemical Geology, 334**, 221–239.

Liu Y., Hou Z.Q., Tian S.H., Zhang Q.C., Zhu Z.M. and Liu J.H. (2015)
Zircon U-Pb ages of the Mianning–Dechang syenites, Sichuan Province, southwestern China: Constraints on the giant REE mineralization belt and its regional geological setting. **Ore Geology Reviews, 70**, 613–636.

Liu Y., Chakhmouradian A.R., Hou Z.Q., Song W.L. and Kynický J. (2018)
Development of REE mineralization in the giant Maoniuping deposit (Sichuan, China): Insights from mineralogy, fluid inclusions, and trace-element geochemistry. **Mineralium Deposita, 54**, 701–718.

Ludwig K.R. (2003)
Isoplot3 – A geochronological toolkit for Microsoft Excel. **Berkeley Geochronology Centre (Berkeley, USA)**, 1–70.

Maluski H. and Matte P. (1984)
Ages of Alpine tectonometamorphic events in the northwestern Himalaya (northern Pakistan) by $^{39}Ar/^{40}Ar$ method. **Tectonics, 3**, 1–18.

McDonough W.F. and Sun S.S. (1995)
The composition of the earth. **Chemical Geology, 120**, 223–253.

McFarlane C.R.M. and McCulloch M.T. (2007)
Coupling of in-situ Sm-Nd systematics and U-Pb dating of monazite and allanite with applications to crustal evolution studies. **Chemical Geology, 245**, 45–60.

McFarlane C.R.M. and McCulloch M.T. (2008)
Sm-Nd and Sr isotope systematics in LREE-rich accessory minerals using LA-MC-ICP-MS. **In: Sylvester P. (ed.), Laser-ablation ICP-MS in the Earth sciences: Current practices and outstanding issues. Mineralogical Association of Canada Short Course, 40**, 117–133.

McLemore V.T. (2010)
Geology and mineral deposit of the Gallinas Mountains, Lincoln and Torrance counties, New Mexico; Preliminary report. **New Mexico Bureau of Geology and Mineral Resources, Open-file Report OF 532**, 92pp.

Mitchell R.H., Wu F.Y. and Yang Y.H. (2011)
In situ U-Pb, Sr and Nd isotopic analysis of loparite by LA-(MC)-ICP-MS. **Chemical Geology, 280**, 191–199.

references

Nakai S., Masuda A. and Lehmann E. (1988)
La-Ba dating of bastnäsite. American Mineralogist, 73, 111–113.

Nakai S., Masuda A., Shimizu H. and Lu Q. (1989)
La-Ba dating and Nd and Sr isotope studies on the Bayan Obo rare earth deposit, Inner Mongolia, China. Economic Geology, 84, 2296–2299.

Nakai S., Halliday A.N., Kesler S.E. and Jones H. (1990)
Rb-Sr dating of sphalerites from Tennessee and the genesis of Mississippi Valley type ore deposits. Nature, 346, 354–357.

Perhac R.M. (1970)
Geology and mineral deposits of the Gallinas Mountains, Lincoln and Torrance Counties, New Mexico. New Mexico Bureau of Mines and Mineral Resources Bulletin, 95, 51–60.

Qureshi A.A., Butt K.A. and Khan H.A. (1991)
Emplacement time of SalaiPatai carbonatite, Malakand, Pakistan, from fission-track dating of zircon and apatite. Nuclear Tracks and Radiation Measurement, 18, 315–319.

Rakovan J., McDaniel D.K. and Reeder R. (1997)
Use of surface-controlled REE sectoral zoning in apatite from Llallagua, Bolivia, to determine a single-crystal Sm-Nd age. Earth and Planetary Science Letters, 146, 329–336.

Ramos F.C., Wolff J.A. and Tollstrup D.L. (2004)
Measuring $^{87}Sr/^{86}Sr$ variation in minerals and groundmass from basalts using LA-MC-ICP-MS. Chemical Geology, 211, 135–158.

Rasoamalala V., Salvi S., Beziat D., Ursule J.P., Cuney M., Parseval P., Guillaume D., Moine B. and Andriamamphihanotona J. (2014)
Geology of bastnäsite and monazite deposit in the Ambatofinanadrahana area, central part of Madagascar: An overview. Journal of African Earth Sciences, 94, 128–140.

Ren Y., Zhang Y. and Zhang Z. (1994)
Study on heat events of ore-forming Bayan Obo deposit. Acta Geosciences Sinica, 15, 95–101. (in Chinese with English abstract)

Robert F. (1990)
Dating old gold deposits. Nature, 346, 792–793.

Romer R.L. and Luders V. (2006)
Direct dating of hydrothermal W mineralization: U-Pb age for hubnerite ($MnWO_4$), Sweet Home Mine, Colorado. Geochimica et Cosmochimica Acta, 70, 4725–4733.

Sal'Nikova E.B., Yakovleva S.Z., Nikiforov A.V., Kotov A.B., Yarmolyuk V.V., Anisimova I.V., Sugorakova A.M. and Plotkina YuV (2010)
Bastnäsite: A promising U-Pb geochronological tool. Doklady Earth Sciences, 430, 134–136.

Scharer U. (1984)
The effect of initial ^{230}Th disequilibrium on young U-Pb ages: The Makalu case, Himalaya. Earth and Planetary Science Letters, 67, 191–204.

Schreiner R.A. (1993)
Mineral investigation of the rare earth element bearing deposits, Red Cloud mining district, Gallinas Mountains, Lincoln County, New Mexico. U.S. Bureau of Mines, Open File Report, 99–93.

Smith H.A. and Giletti B.J. (1997)
Lead diffusion in monazite. Geochimica et Cosmochimica Acta, 61, 1047–1055.

Soman A., Geisler T., Tomaschek F., Grange M. and Berndt J. (2010)
Alteration of crystalline zircon solid solutions: A case study on zircon from an alkaline pegmatite from Zomba-Malosa, Malawi. Contributions to Mineralogy and Petrology, 160, 909–930.

Stacey J.S. and Kramers J.D. (1975)
Approximation of terrestrial lead isotope evolution by a two-stage model. Earth and Planetary Science Letters, 26, 207–221.

Tian J.X., Zhang R.T., Fan Y.C., Li X.Z., Xu H.Y. and Wang B.Y. (2002)
Geological characteristics and relation with rare earth elements of alkali complex in Chishan of Shandong Province. Land Resource Shandong Province, 18, 21–25. (in Chinese with English abstract)

Tian S.H., Hou Z.Q., Yang Z.S., Chen W., Yang Z.M., Yuan Z.X., Xie Y.L., Fei H.C., Yin S.P., Liu Y.C., Li Z. and Li X.Y. (2008)
Geochronology of REE deposits from the Mianning-Dechang REE belt: Constraints on the duration of hydrothermal activities and a tectonic model for the carbonatite-alkalic complexes in Sichuan, SW China. Mineral Deposits, 27, 177–187. (in Chinese with English abstract)

Vroon P.Z., van der Wagt B., Koornneef J.M. and Davies G.R. (2008)
Problems in obtaining precise and accurate Sr isotope analysis from geological materials using laser ablation MC-ICP-MS. Analytical and Bioanalytical Chemistry, 390, 465–476.

Wang J., Tatsumoto M., Li X., Premo W.R. and Chao E.C.T. (1994)
A precise ^{232}Th-^{208}Pb chronology of fine-grained monazite: Age of the Bayan Obo REE-Fe-Nb ore deposit, China. Geochimica et Cosmochimica Acta, 58, 3155–3169.

Weis D., Kieffer B., Maerschalk C., Pretorius W. and Barling J. (2005)
High-precision Pb-Sr-Nd-Hf isotopic characterization of USGS BHVO-1 and BHVO-2 reference materials. Geochemistry, Geophysics, Geosystems, 6, Q02002. https://doi.org/10.1029/2004GC000852.

references

Weis D., Kieffer B., Maerschalk C., Barling J., Jong J.D., Williams G.A., Hanano D., Pretorius W., Mattielli N., Scoates J.S., Goolaerts A., Friedman R.M. and Mahoney J.B. (2006)
High-precision isotopic characterization of USGS reference materials by TIMS and MC-ICP-MS. Geochemistry, Geophysics, Geosystems, 7, Q08006. https://doi.org/10.1029/2006GC001283.

Williams I.S.(1998) U
-Th-Pb geochronology by ion microprobe. In: McKibben M.A., Shanks W.C. and Ridley W.I. (eds), Reviews in Economic Geology, 7, 1–35.

Williams-Jones A.E., Samson I.M. and Ollivo G.R. (2000)
The genesis of hydrothermal of fluorite-REE deposits in the Gallinas Mountains, New Mexico. Economic Geology, 95, 327–342.

Woodhead J., Swearer S., Hergt J. and Maas R. (2005)
In situ Sr-isotope analysis of carbonates by LA-MC-ICP-MS: Interference corrections, high spatial resolution and an example from otolith studies. Journal of Analytical Atomic Spectrometry, 20, 22–27.

Wu F.Y., Yang Y.H., Xie L.W., Yang J.H. and Xu P. (2006)
Hf isotopic compositions of the standard zircons and baddeleyites used in U-Pb geochronology. Chemical Geology, 234, 105–126.

Wu F.Y., Yang Y.H., Bellatreccia F., Mitchell R.H. and Li Q.L. (2010a)
In situ U-Pb and Sr-Nd-Hf isotopic investigations of zirconolite and calzirtite. Chemical Geology, 277, 178–195.

Wu F.Y., Yang Y.H., Michael A.W.M., Liu Z.C., Zhou Q., Ge W.C., Yang J.S., Zhao Z.F., Mitchell R.H. and Markl G. (2010b)
In situ U-Pb, Sr, Nd and Hf isotopic analysis of eudialyte by LA-(MC)-ICP-MS. Chemical Geology, 273, 8–34.

Wu F.Y., Yang Y.H., Mitchell R.H., Li Q.L., Yang J.H. and Zhang Y.B. (2010c)
In situ U-Pb age determination and Nd isotopic analysis of perovskites from kimberlites in southern Africa and Somerset Island, Canada. Lithos, 115, 205–222.

Xu C., Campbell I.H., Kynicky J., Allen M.C., Chen Y.J., Huang Z.L. and Qi L. (2008)
Comparison of the Daluxiang and Maoniuping carbonatitic REE deposits with Bayan Obo REE deposits, China. Lithos, 106, 12–24.

Xu C., Kynicky J., Chakhmouradian A.R., Campbell I.H. and Allen C.M. (2010)
Trace-element modeling of the magmatic evolution of the rare-earth-rich carbonatite from the Miaoya deposit, Central China. Lithos, 118, 45–155.

Xu C., Taylor R.N., Li W., Kynicky J., Chakhmouradian A.R. and Song W. (2012)
Comparison of fluorite geochemistry from REE deposits in the Panxi region and Bayan Obo, China. Journal of Asian Earth Sciences, 57, 76–89.

Xu C., Chakhmouradian A.R., Taylor R.N., Kynicky J., Li W.B., Song W.L. and Fletcher I.R. (2014)
Origin of carbonatites in the South Qinling orogen: Implication for crustal recycling and timing of collision between the South and North China Blocks. Geochimica et Cosmochimica Acta, 143, 189–206.

Xu C., Kynicky J., Chakhmouradian A.R., Li X.H. and Song W.D. (2015)
A case example of the importance of multi-analytical approach in deciphering carbonatite petrogenesis in South Qinling orogen: Miaoya rare-metal deposit, central China. Lithos, 227, 107–121.

Yang G.M., Chang C., Zuo D.H. and Liu X.L. (1998)
Geology and mineralization of the Dalucao REE deposit in Dechang County, Sichuan Province. Published File of China University of Geosciences (Wuhan), 1–89. (in Chinese with English abstract)

Yang Y.H., Sun J.F., Xie L.W., Fan H.R. and Wu F.Y. (2008)
In situ Nd isotopic measurement of natural geological materials by LA-MC-ICP-MS. Chinese Science Bulletin, 53, 1062–1070.

Yang Y.H., Wu F.Y., Fan H.R., Xie L.W. and Zhang Y.B. (2009a)
In situ Nd isotope measurement of bastnäsite via LA-MC-ICP-MS. Geochimica et Cosmochimica Acta, 73, A1481.

Yang Y.H., Wu F.Y., Wilde S.A., Liu X.M., Zhang Y.B., Xie L.W. and Yang J.H. (2009b)
In situ perovskite Sr-Nd isotopic constraints on the petrogenesis of the Ordovician Mengyin kimberlites in the North China Craton. Chemical Geology, 264, 24–42.

Yang Y.H., Wu F.Y., Xie L.W., Yang J.H. and Zhang Y.B. (2009c)
In situ Sr isotopic measurement of natural geological samples by LA-MC-ICP-MS. Acta Petrologica Sinica, 25, 3431–3441. (in Chinese with English abstract)

Yang Y.H., Wu F.Y., Xie L.W. and Zhang Y.B. (2010a)
High-precision measurements of the $^{143}Nd/^{144}Nd$ isotope ratio in certified reference materials without Nd and Sm separation by multiple collector inductively coupled plasma-mass spectrometry. Analytical Letters, 43, 142–150.

Yang Y.H., Zhang H.F., Chu Z.Y., Xie L.W. and Wu F.Y. (2010b)
Combined chemical separation of Lu, Hf, Rb, Sr, Sm and Nd from a single rock digest and precise and accurate isotope determinations of Lu-Hf, Rb-Sr and Sm-Nd isotope systems using multi-collector ICP-MS and TIMS. International Journal of Mass Spectrometry, 290, 120–126.

Yang Y.H., Chu Z.Y., Wu F.Y., Xie L.W. and Yang J.H. (2011a)
Precise and accurate determination of Sm, Nd concentrations and Nd isotopic compositions in geological samples by MC-ICP-MS. Journal of Analytical Atomic Spectrometry, 26, 1237–1244.

references

Yang K.F., Fan H.R., Santosh M., Hu F.F. and Wang K.Y. (2011b)
Mesoproterozoic carbonatitic magmatism in the Bayan Obo deposit, Inner Mongolia, North China: Constraints for the mechanism of super accumulation of rare earth elements. **Ore Geology Reviews, 40**, 122–131.

Yang Y.H., Wu F.Y., Xie L.W., Yang J.H. and Zhang Y.B. (2011c)
High-precision direct determination of the $^{87}Sr/^{86}Sr$ isotope ratio of bottled Sr-rich natural mineral drinking water using multiple collector inductively coupled plasma-mass spectrometry. **Spectrochimica Acta Part B, 66**, 656–660.

Yang Y.H., Wu F.Y., Liu Z.C., Chu Z.Y., Xie L.W. and Yang J.H. (2012)
Evaluation of Sr chemical purification technique for natural geological samples using common cation exchange and Sr-specific extraction chromatographic resin prior to MC-ICP-MS or TIMS measurement. **Journal of Analytical Atomic Spectrometry, 27**, 516–522.

Yang Y.H., Wu F.Y., Chu Z.Y., Xie L.W. and Yang J.H. (2013)
High-precision simultaneous determination of $^{147}Sm/^{144}Nd$ and $^{143}Nd/^{144}Nd$ ratios in Sm-Nd mixtures using multi-collector inductively coupled plasma-mass spectrometry and its comparison to isotope dilution analysis. **Spectrochimica Acta Part B, 79–80**, 82–87.

Yang Y.H., Wu F.Y., Li Y., Yang J.H., Xie L.W., Liu Y., Zhang Y.B. and Huang C. (2014a)
In situ U-Pb dating of bastnäsite by LA-ICP-MS. **Journal of Analytical Atomic Spectrometry, 29**, 1017–1023.

Yang Y.H., Wu F.Y., Yang J.H., David M.C., Xie L.W., Chu Z.Y., Zhang Y.B. and Huang C. (2014b)
Sr and Nd isotopic compositions of apatite reference materials used in U-Th-Pb geochronology. **Chemical Geology, 385**, 35–55.

Yuan Z.X., Shi Z.M., Bai G., Wu C.Y., Chi R.A. and Li X.Y. (1995)
The maoniuping rare earth ore deposit, Mianning County, Sichuan Province. **Seismological Press (Beijing)**, 150pp. (in Chinese with English abstract)

Zhang Z.Q., Yuan Z.X., Tang S.H., Bai G. and Wang J.H. (2003)
Age and geochemistry of the Bayan Obo ore deposit. **Geological Publishing House (Beijing)**, 222pp. (in Chinese with English abstract)

Zhang S.H., Zhao Y. and Liu Y.S. (2017)
A precise zircon Th-Pb age of carbonatite sills from the world's largest Bayan Obo deposit: Implication for timing and genesis of REE-Nb mineralization. **Precambrian Research, 291**, 202–219.

Zhao Z.F. and Zheng Y.F. (2007)
Diffusion compensation for argon, hydrogen, lead, and strontium in minerals: Empirical relationships to crystal chemistry. **American Mineralogist, 92**, 289–308.

Supporting information

The following supporting information may be found in the online version of this article:

Table S1. Major and trace element compositions of bastnäsite samples.

Table S2. *In situ* U-Th-Pb bastnäsite age data.

Table S3. *In situ* Rb-Sr bastnäsite isotopic data.

Table S4. *In situ* Sm-Nd bastnäsite isotopic data.

Appendix S1. Sample descriptions.

This material is available from: http://onlinelibrary.wiley.com/doi/10.1111/ggr.12297/abstract (This link will take you to the article abstract).